# Acoustic Impedance of a Bb Trumpet

David T. Pignotti

January 23, 2008

## Abstract

A phase-sensitive method is developed to measure the complex input and output impedance spectrums of a reed-driven instrument using a computer-based data acquisition system. The system is comprised of a sine wave function generator, a piezoelectric transducer to excite the air within the instrument, the world's smallest microphone to measure pressure, miniature custom-built differential pressure microphones to measure air particle velocity, four lock-in amplifiers, and eight ADCs on a data-acquisition card. These same components of pressure and particle velocity enable the determination of not only the complex input and output impedance, but also the complex sound intensity of the instrument and, more generally, for any vibrating air column as well as free air. The input impedance spectrum of a reed-driven instrument gives information on which notes an instrument can produce and the relative difficulty a player encounters when playing a specific note, the output impedance spectrum gives information on what is heard by a listener.

# I. Introduction

There are two different types of wind instruments, those that exhibit low or high input impedance at the point at which a player excites the air flowing through the instrument. The low-impedance group refers to instruments such as the flute, organ pipe, or recorder. The technique presented here involves measuring the input impedance of the high impedance group—reed driven instruments (both wooden reeds or lip "reeds") such as the clarinet, saxophone, or trumpet.[1] This paper focuses specifically on the input and output impedances of a trumpet, however the method can easily be applied to any musical instrument, as well as to any arbitrary sound field.

When a player's lips excite the air that is forced through a trumpet, the air resonates at the natural frequency of the tube in which the air flows. In the case of the trumpet, the tube appears to be open—at the mouthpiece and at the bell. Thus the trumpet would be expected to produce the fundamental frequency associated with the ~147-cm tube length ($f_0 \approx 117$ Hz, $C_3$) and all the subsequent even and odd harmonics ($C_4$, $G_4$, $C_5$, $E_5$, $G_5$, a flat $B_{b5}$ and $C_6$) when no valves are pressed.[2] This model agrees with the notes that can actually be played when all three of the valves are open. However, even though the tubing of a trumpet is open, there is such a large frequency-dependent impedance mismatch at the bell end of the trumpet that the tubing behaves as if it is effectively closed at that end. When a trumpet is played, the player's lips are closed at the input end of the instrument the majority of the time. The lips open only to allow a short burst of air into the trumpet tubing. Since the player's lips are significantly stiffer than the surrounding free air, the input at the mouthpiece of the instrument is closed. Thus the trumpet is a closed-closed system, not an open-open or open-closed system as one might

naively think. Similar to the faux open-open system, the actual closed-closed system trumpet produces the fundamental frequency and all the subsequent even and odd harmonics, but these are closed-closed harmonics, not open-open.

If a musician compares a professional-grade instrument to a beginner instrument, he/she will find that even though the instruments are almost identical, the professional instrument will sound much better and be much easier to play. The tone quality and tuning of an instrument is determined by the input impedance spectrum of the instrument. By measuring the acoustical input impedance spectrum, we can see what notes are produced by a musical instrument and the relative ease of playing a specific note without actually playing the instrument.

## II. Background

Acoustical input impedance is defined as a measure of resistance to putting a pressure wave through a tube.[3] The quotient of the complex pressure wave and the complex air particle velocity at a point $r$ inside the inside the instrument gives the value of the complex specific acoustic impedance at that point:

$$\tilde{Z}(\boldsymbol{r}) = \frac{\tilde{P}(\boldsymbol{r})}{\tilde{\boldsymbol{U}}(\boldsymbol{r})}.$$

The SI units of specific acoustic impedance (hereafter called impedance) are Pa·s/m (= kg/m$^2$·s) or simply "acoustical ohms." When a trumpet is played, the player's lips vibrate, injecting bursts of air and pressure into the trumpet tubing. The pressure wave travels through the trumpet and is reflected back towards the mouthpiece where it encounters a sharp change of the radius of the tube at the bell end of the trumpet

(Figure 1). The reflected pressure wave gives the player's lips "information" on the frequency at which to vibrate. Therefore, the higher the impedance, the greater amount of pressure waves reflected, and thus the easier it is to play that note.[3] This phenomenon allows the trumpet to sound a desired note with ease.

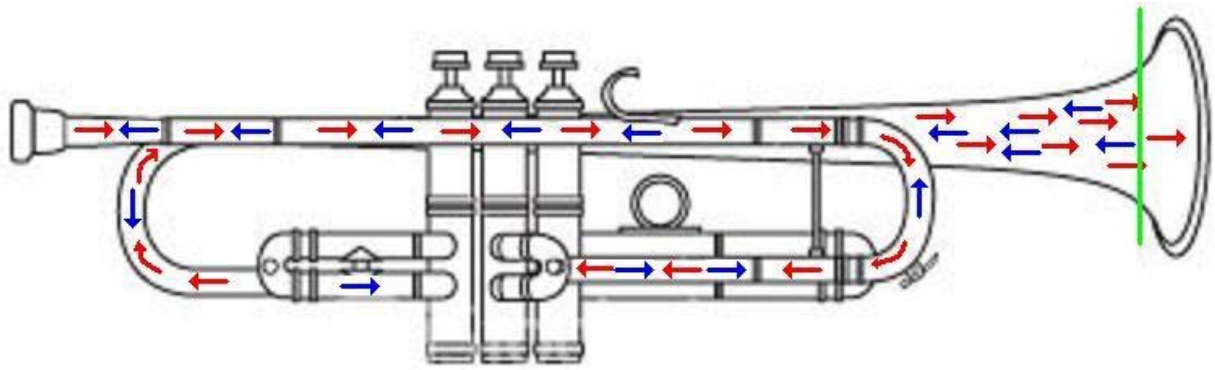

*Figure 1. Schematic of pressure and air flow through a trumpet. When the instrument is excited, air particles and pressure waves (red arrows) travel through the tubing of the trumpet. When the pressure waves encounter a large impedance mismatch (green line), the waves (blue arrows) are reflected back to the player's lips, giving vibrating frequency information.*

Backus investigated the change in the input impedance spectrum throughout the various stages of the construction of a trumpet.[4] The lowest mode is actually the second harmonic, since the fundamental frequency for brass instruments cannot be easily played. Because of the construction of the mouthpiece, which favors the higher harmonics, the fundamental frequency is available only to extremely experienced players. Nevertheless, the trumpet is driven by the player's lips at the fundamental frequency; thus higher harmonics appear at integer multiples of the fundamental. Figure 2 shows the input impedance peaks throughout different stages of assembly of a trumpet. The cylindrical tubing alone shows a steady decrease in the magnitude of the input impedance peaks as

frequency increases, but the peaks do not line up with the desired note frequencies for a trumpet. When the bell is added, the input impedance peaks still steadily decrease but the higher modes decrease more rapidly than they did without the bell. The bell also matches the input impedance peaks with the desired frequencies better than with the tubing alone. The tubing plus mouthpiece and leader pipe show a steady increase of the input impedance peaks of the modes as frequency increases and then displays a sharp falloff after about the eighth harmonic. The input impedance peaks are somewhat better matched to the desired frequencies. When the bell is added to this third system, the input impedance peaks shift to almost exactly the frequencies required for a trumpet.[4]

Figure 3 shows the discrepancies between the $n^{th}$ resonance and the $n^{th}$ harmonic throughout the stages of assembly of a trumpet. Before the instrument is put together, the deviation from the resonances and the harmonics for the cylindrical tubing at the fifth mode is one-fourth an octave. When the bell is added, the deviation at the fifth mode is one-sixth an octave. When the mouthpiece is added, the deviation is lowered to one-twelfth of an octave. Finally, when the instrument is complete, no appreciable deviation from desired harmonics occurs.[4]

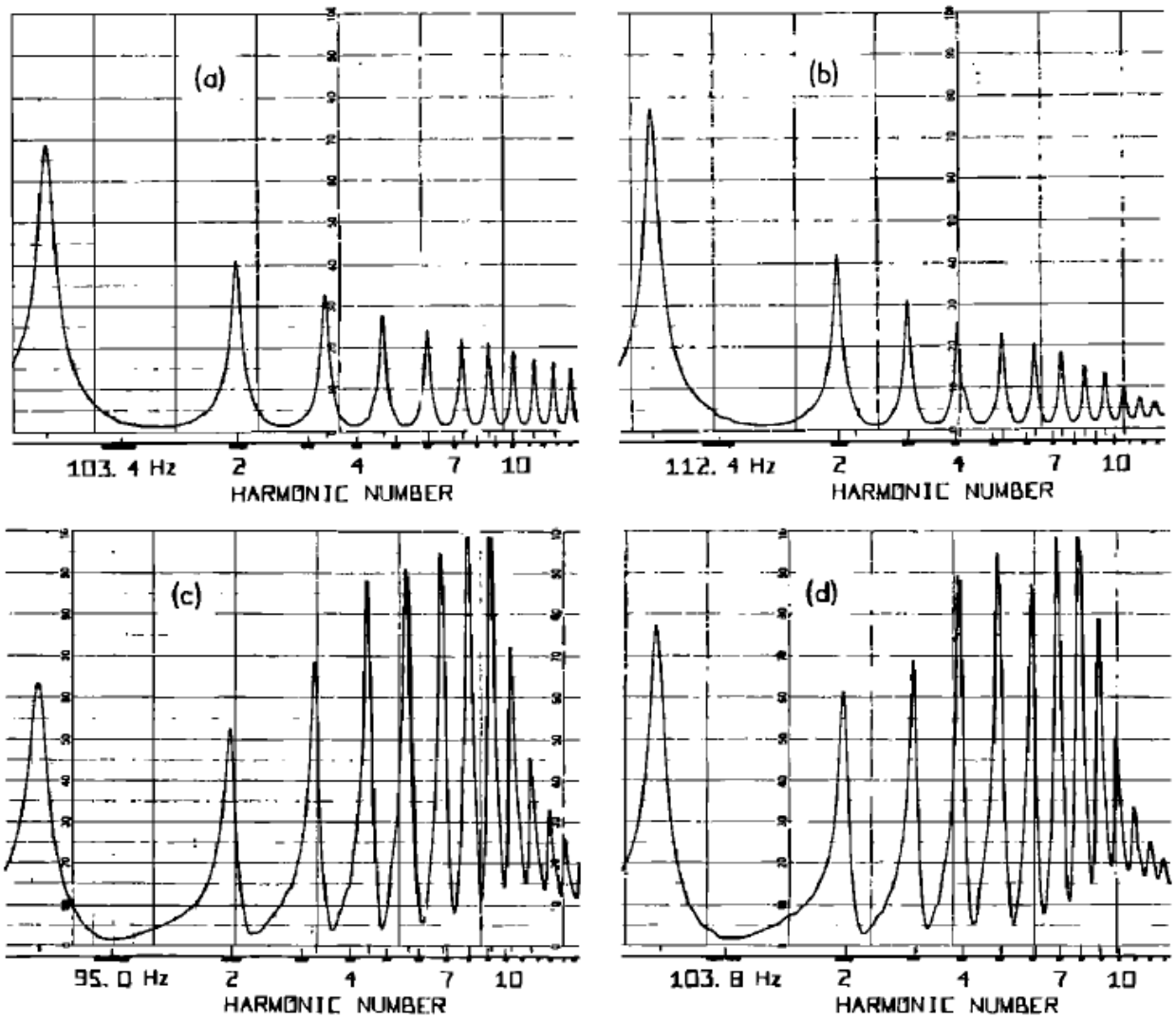


*Figure 2. Input impedance curves for the construction of a modern Bb trumpet. (a) a length of cylindrical tubing; (b) tubing plus trumpet bell; (c) tubing plus mouthpiece and leader pipe; and (d) tubing plus bell plus mouthpiece and leader pipe. Full scale is 1000 acoustic Ω (CGS)[*] or 10000 acoustic Ω (MKS). Note: This plot is taken from J. Backus, J.Acoust. Soc. Am. 60, 1266 (1976).*[4]

[*] *1Ω (CGS) = 1 barye-second/cm = 0.1 Pascal-second/0.01 meter = 10 Pascal-second/meters = 10 Ω (MKS).*

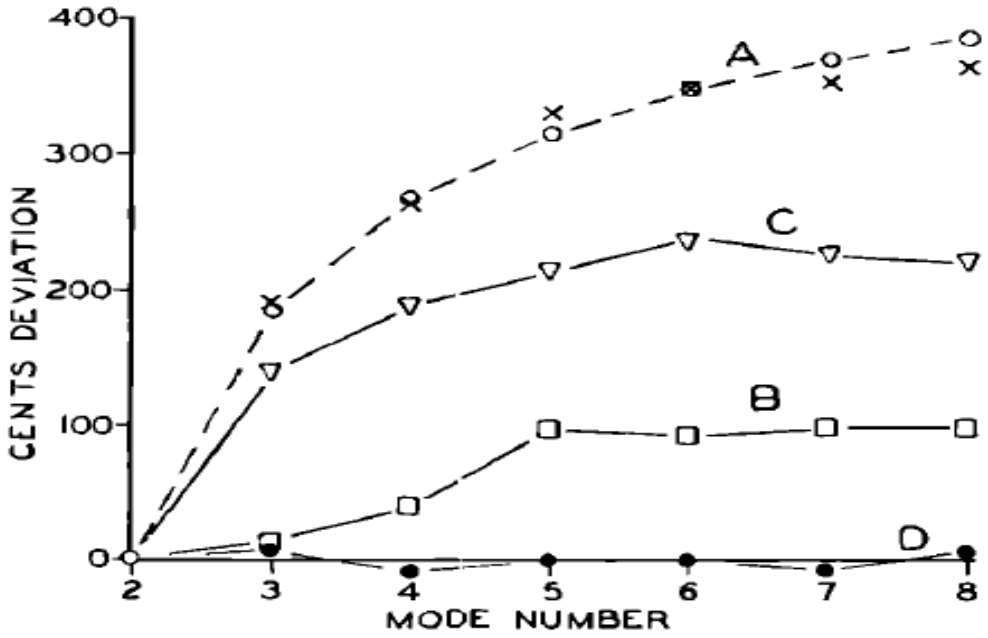


*Figure 3. Plots of the discrepancies in cents between the $n^{th}$ resonance and the $n^{th}$ harmonic, with the second resonance coinciding with the second harmonic. (a) Cylindrical tubing; (b) tubing plus bell; (c) tubing plus leader pipe and mouthpiece; and (d) tubing plus bell plus leader pipe and mouthpiece. This plot is taken from J. Backus, J.Acoust. Soc. Am. 60, 1266 (1976).*[4]

To measure the complex input impedance of an instrument, Benade developed a piezo-disk-driven impedance head apparatus.[5] This technique involves attaching a piezo-transducer onto the mouthpiece of the instrument. Benade states that if the stiffness of the piezoelectric disk is large compared to the highest possible input impedance of the air column under study, then the acoustical pressure observed at the input end of the air column is an accurate measure of the air column's own input impedance. He further states that this measurement of the air column's input impedance is accurate as long as the frequency at which the tube is excited is not a resonant frequency of the piezo-transducer. A microphone is inserted into the mouthpiece near the piezo-transducer to measure the pressure response to the voltage-dependent oscillations provided by the transducer. Benade states that his microphone has a flat frequency response from 50 Hz to 5000 Hz. The air particle velocity, Benade claims, is related to the amount of air displaced by the vibrations of the piezo transducer. Using the pressure and calculated air particle velocity values, Benade calculated the acoustical impedance of a trumpet over a range of frequencies.[5]

In this paper, a new and improved phase-sensitive technique is devised for measuring the complex input impedance by directly measuring the air particle velocity using a modified differential pressure microphone.

## III. Experimental Apparatus

The specific acoustical input impedance of the trumpet was measured using a piezoelectric driver, two 1/10″ Knowles Acoustics FG-23329 high-performance omni-directional microphone (KAP) to measure internal and external pressure, a modified

Knowles Acoustics EK-23132 high performance omni-directional microphone (KAU) to measure internal particle velocity, and a modified RadioShack 270-090 condenser microphone (RSU) to measure external particle velocity. While the RSU is just as effective in measuring particle velocity as the KAU microphone, the KAU mic is much smaller which allows insertion into much smaller places such as the mouthpiece of a trumpet. A KAP pressure microphone and a KAU microphone were mounted inside the mouthpiece near the piezo-transducer to determine the input impedance. In order to install the miniature pressure and particle-velocity microphones inside the trumpet mouthpiece, two small holes were drilled on either side of the mouthpiece. Since the pressure microphone is omni-directional, the orientation of the microphone inside the mouthpiece was arbitrary. However, the omni-directionality of the Knowles Acoustics EK-23132 microphone was destroyed when it was modified. Thus knowledge of the orientation of the particle-velocity microphone inside the mouthpiece is essential to get proper magnitude measurements. The plane of the miniature particle-velocity microphone must be perpendicular to the expected air flow. After both microphones were mounted into the trumpet mouthpiece, a wafer-thin 1" diameter piezo-transducer was rigidly attached to the opening of the trumpet mouthpiece using cyanoacrylate glue (Figure 4). The remaining KAP and RSU microphones were placed outside the trumpet in the plane of the bell along the direction of airflow to measure external output pressure and particle velocity respectively. As with the values of the input pressure and particle velocity, these output values define the output impedance of the trumpet.

During later runs of the experiment, the external KAP and RSU microphones were placed outside the mouthpiece in proximity to the piezo transducer to detect

potential coupling of the internal pressure and particle velocity of the instrument with the free air at the mouthpiece of the instrument.

The room in which these measurements were carried out suffered from *1/f* noise associated with the ventilation system. To improve the signal-to-noise ratio, the entire trumpet, microphones, and associated preamp electronics were placed inside a large acoustically damped wooden box (Figure 5).

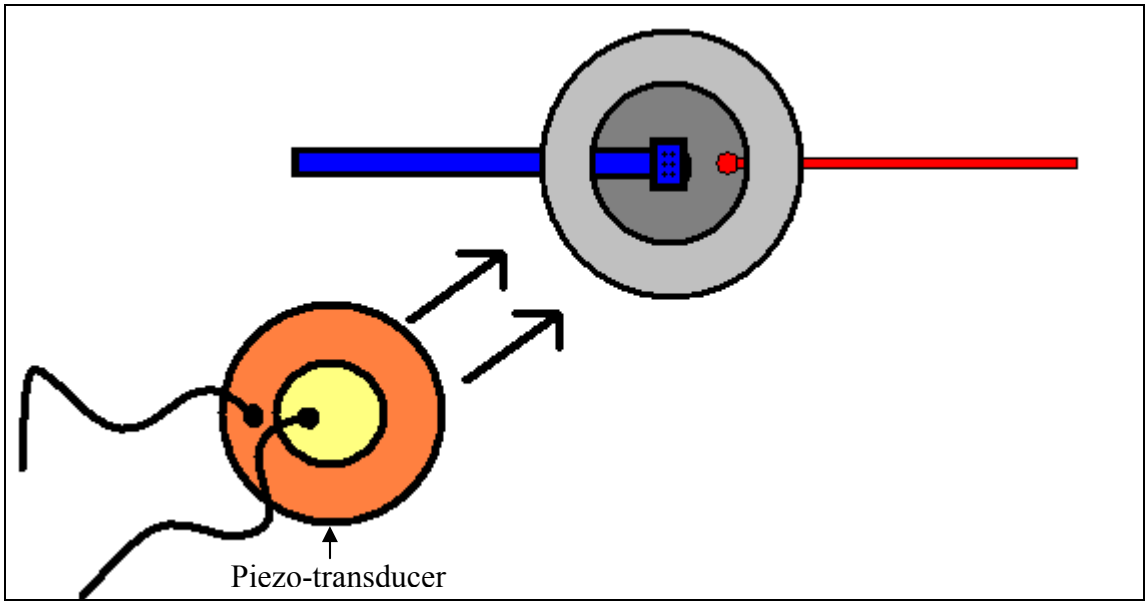


*Figure 4. The Knowles Acoustics EK- 23132 particle-velocity microphone (blue) and the Knowles Acoustics FG-23329 pressure microphone (red), inserted through two small holes on the perimeter of the mouthpiece. Once the particle-velocity microphone is properly aligned perpendicular to the airflow, the piezo-transducer is rigidly attached to the mouth-opening of the mouthpiece with cyanoacrylate glue.*

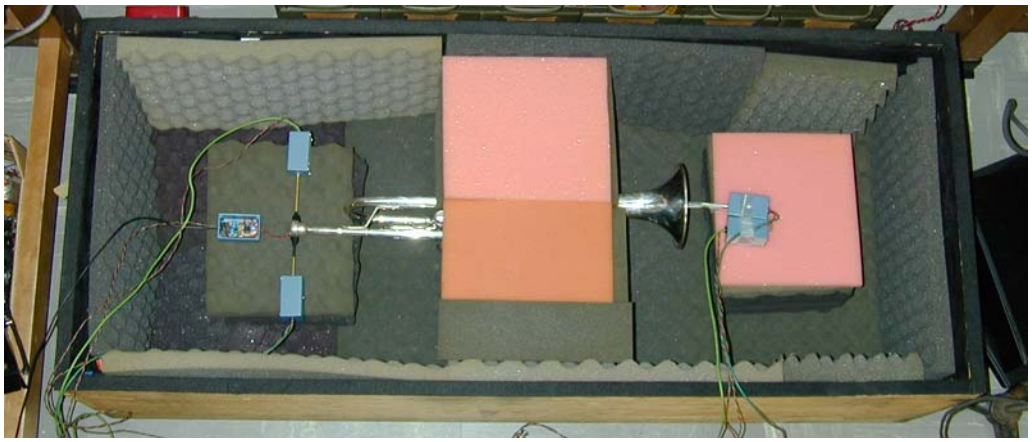

*Figure 5. Trumpet, microphones, and associated preamp electronics inside a large acoustically damped wooden box. External microphones are placed in the plane of the trumpet bell along the direction of airflow.*

The Knowles Acoustics FG-23329 omni-directional microphone used to measure the pressure is 0.1" in diameter. It was chosen because of its small size and its flat frequency response up to 10,000 Hz. Keeping the components inside the instrument's mouthpiece as small as possible is important so as to minimally disturb the air volume of the mouthpiece and ensure negligible disruption of airflow. The Knowles Acoustics pressure microphones were each connected to custom built preamps (Figure 6) to increase the microphone's voltage output before being fed into lock-in amplifiers. Plots of the voltage gain vs. frequency and the phase vs. frequency of the Knowles Acoustics pressure microphone preamplifiers are shown in Figure 7. The voltage gain of this preamp is flat up to 1.0 MHz, while the phase stays constant up to 40.0 kHz, both of which are well over the audio frequency range.

The particle-velocity microphone used for the external particle-velocity measurement was made from a modified RadioShack type 270-090 electret condensor microphone identical to one used to measure the internal particle velocity of a tenor saxophone in an earlier experiment.[6] The design of the modification of this microphone

was introduced by Bennet-Clark in his paper concerning the measurement of air particle velocity produced by small insects.[7] The modified microphone components are a pressure-gradient transducer, a field-effect transistor (FET) impedance converter, and a fine copper mesh screen used for shielding the interior components of the microphone from exterior sources of electromagnetic noise as well as protecting the pressure-gradient transducer from damage due to dust.

The particle-velocity microphone used for the trumpet mouthpiece was made from a modified Knowles Acoustics EK-23132 high performance, omni-directional microphone very similar to the "first generation" RadioShack condenser microphone, but much smaller. The same modification method discussed by Bennet-Clark and previously applied to the RadioShack microphones were used for the new, smaller KAU microphone.[7]

Additional technical details of all microphones used in the experiment are contained in Appendix I.

Once the differential pressure signal is obtained from either microphone, via use of the 1-D version of Euler's equation for inviscid fluid flow,

$$\rho_0 \frac{\partial \mathbf{U}_z(z,t)}{\partial t} = -\frac{\partial P(z,t)}{\partial z}$$

the time-integral of the differential pressure signal produces a value linearly proportional to the particle velocity:

$$u_z(z,t) = -\frac{1}{\rho_o}\int_{-\infty}^{t} \frac{\partial p(z,t')}{\partial z}\, dt' \quad ,$$

where $\rho_o \simeq 1.2\,kg/m^3$ is the ambient density of air at NTP. Note that $\frac{\partial p}{\partial z}$ produces a signal that is linearly proportional to frequency.

The integration is accomplished by routing the signal from the particle-velocity sensor through a custom-built integrating preamp (Figure 8) before it is connected to the lock-in amplifier. The integrating op amp has a frequency response linearly proportional to *1/f* thus, the frequency response of the combined particle-velocity microphone and integrating amplifier is flat in the audio frequency range of interest (100—3000 Hz), and the phase response is constant to within 10° over this same frequency range. Plots of the voltage gain vs. frequency and the phase vs. frequency of the integrating preamplifier are shown in Figure 9. The voltage gain of the preamp decreases logarithmically with frequency, whereas the differential microphone output increases logarithmically over this same frequency range from 10 Hz to 10 kHz.

The piezo-transducer that excites the air in the instrument is driven by a computer-controlled Agilent 33220A function generator. The driving voltage passes through a custom-built voltage amplifier (Figure 10) to boost the driving voltage by a factor of 10×. Plots of the voltage gain vs. frequency and the phase vs. frequency of the voltage amplifier are shown in Figure 11. The voltage amplifier induces a phase shift greater than 5° beyond ~20 kHz, but since the frequency range of interest for the trumpet is below 2000 Hz, this phase shift can be ignored.

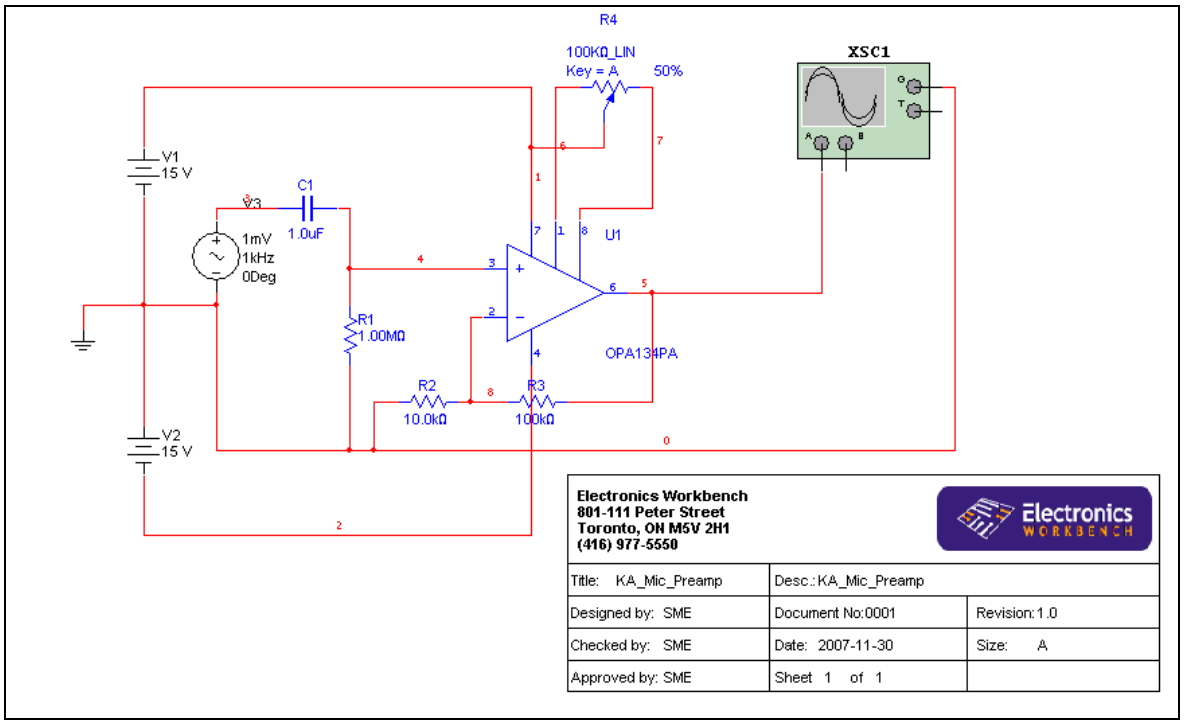


*Figure 6. Schematic of the Knowles Acoustics pressure microphone preamplifier. The OPA134PA op-amp amplifies the microphone voltage by a factor of 11x.*

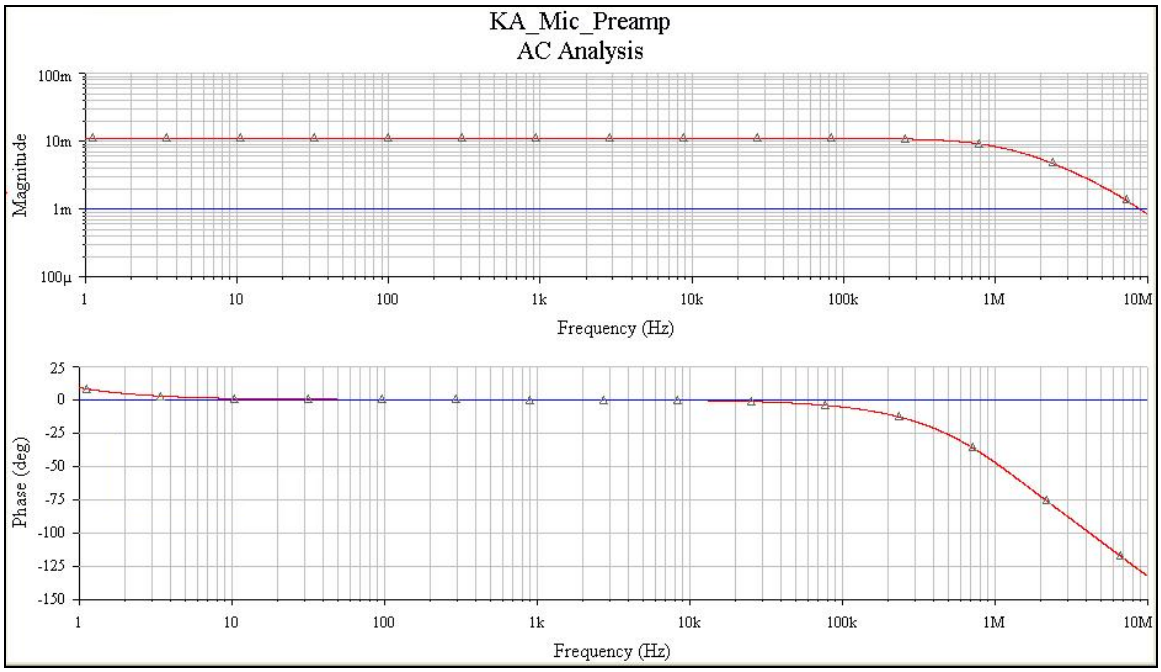


*Figure 7. Voltage gain and phase plots of the pressure microphone preamplifiers on a logarithmic frequency scale. The red line represents the output of the preamplifiers.*

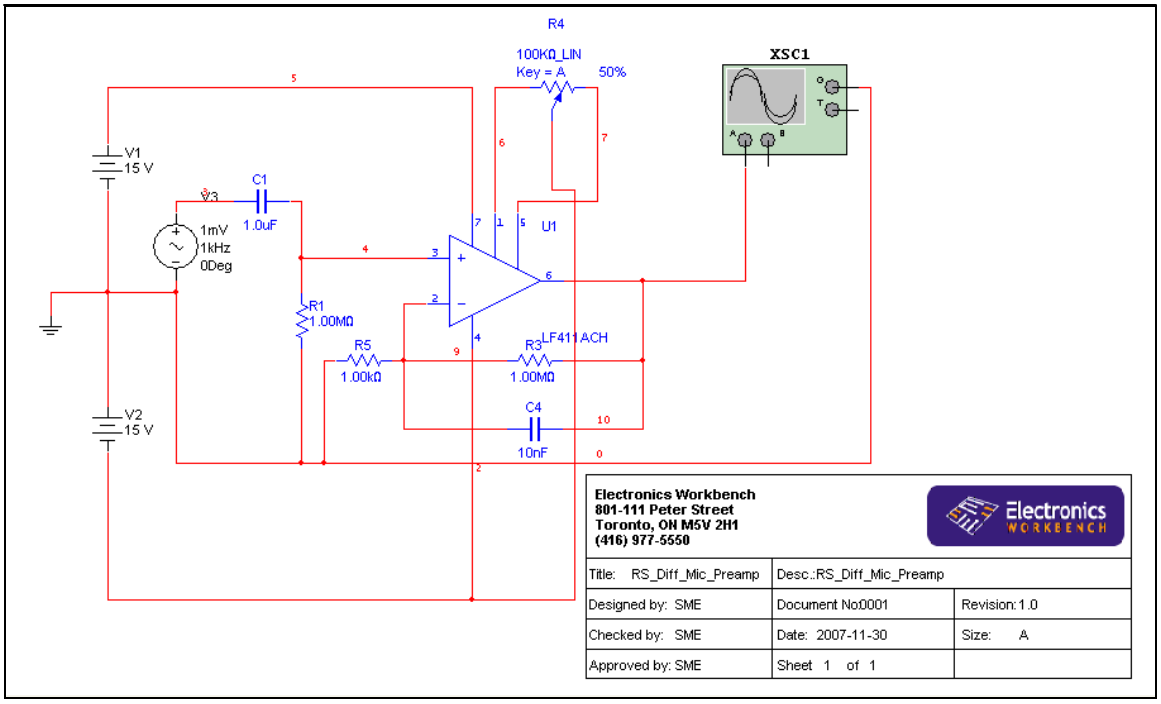


*Figure 8. Integrating preamp circuit integrates the differential pressure signal from the particle-velocity microphone when the instrument is being driven.*

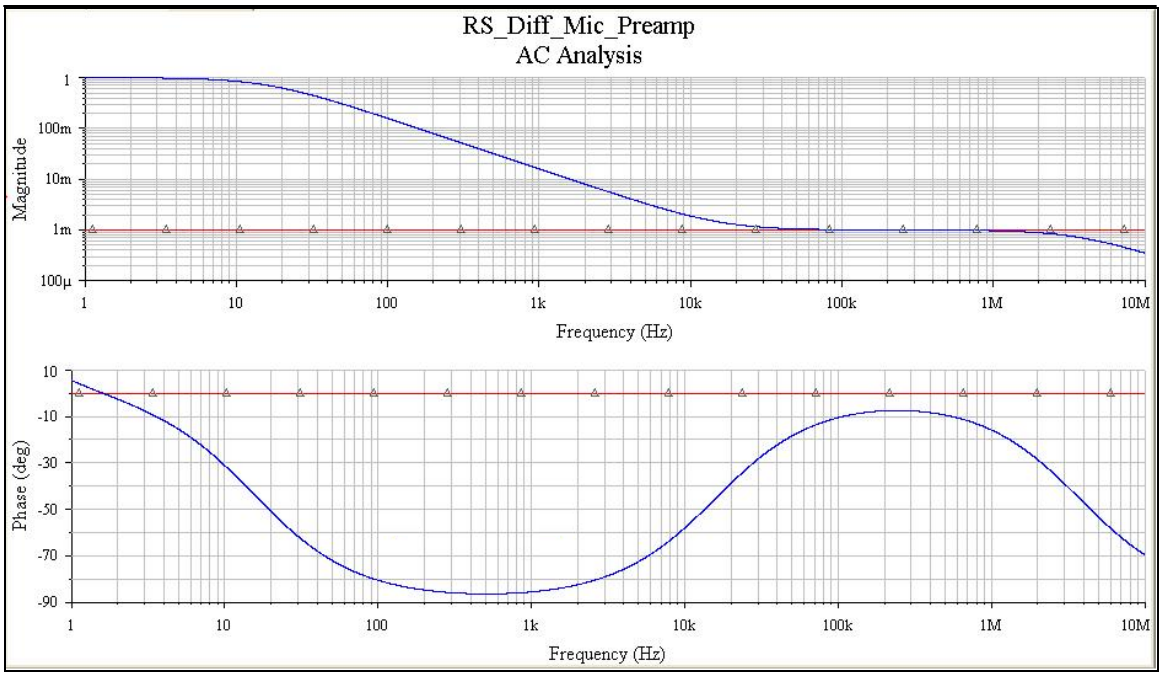


*Figure 9. Voltage gain and phase plots of the differential pressure particle-velocity microphone integrating preamplifiers on a logarithmic frequency scale. The blue line represents the output of the preamplifiers.*

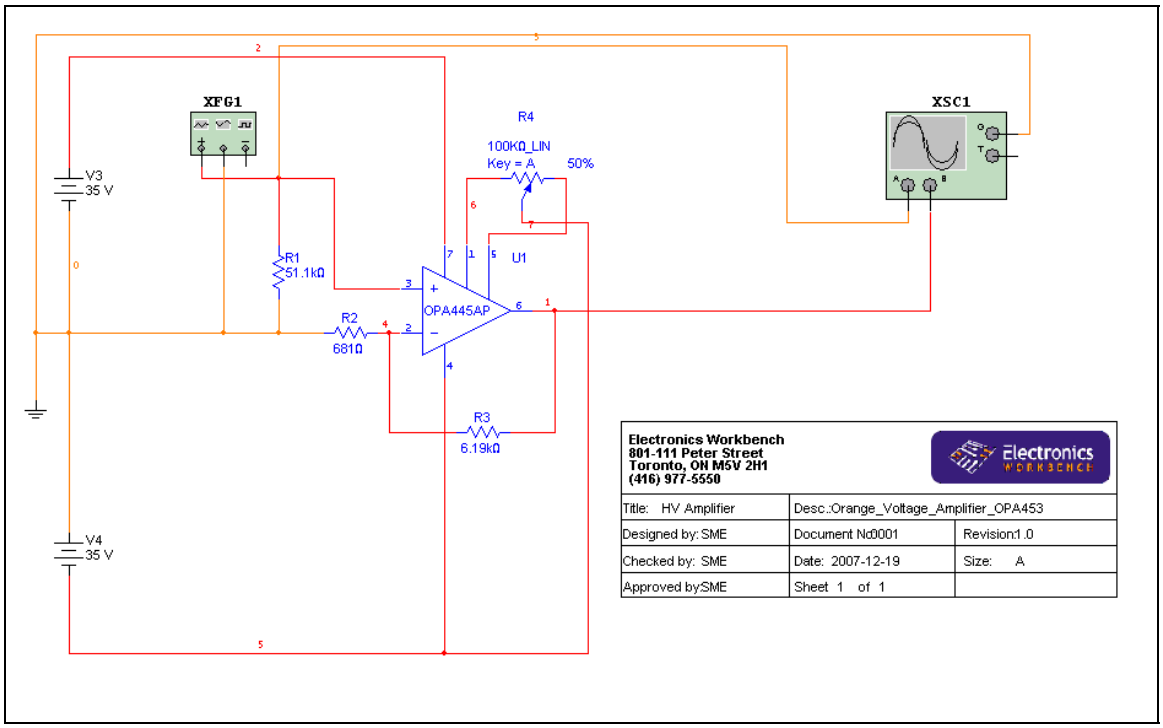


*Figure 10. The voltage amplifier increases the voltage output from the function generator to the piezo-transducer resulting in a 10× increase in amplitude relative to that where the transducer was driven with the function generator alone.*

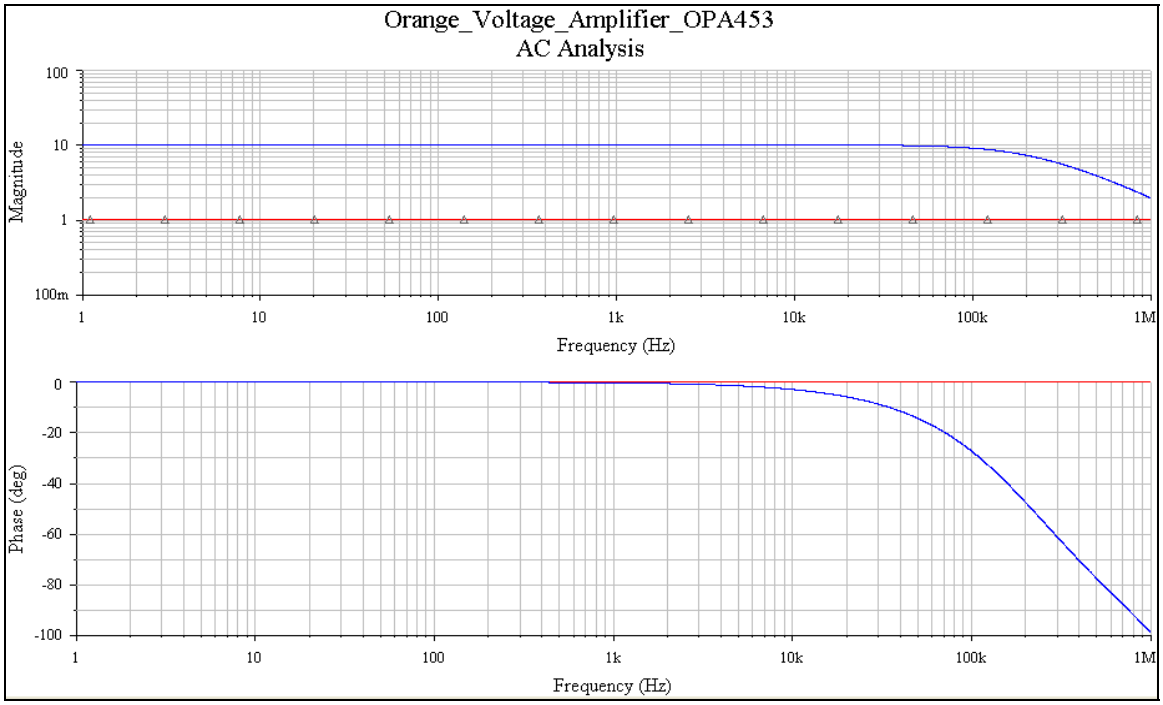


*Figure 11. Voltage gain and phase plots of the voltage amplifier on a logarithmic frequency scale. The red line represents the output of the preamplifier. While a phase shift > 5$^{o}$ is introduced after ~20,000 Hz, it is negligible in the frequency range of interest for a trumpet.*

The driving voltage from the voltage amplifier then passes through a negative impedance converter (NIC) circuit (Figure 12) to provide the piezo-transducer with true constant current and a phase shift of –90° over the full range of interest in the audio frequency band. Plots of the voltage gain vs. frequency and the phase vs. frequency of the NIC-constant-current driven circuit are shown in Figure 13.

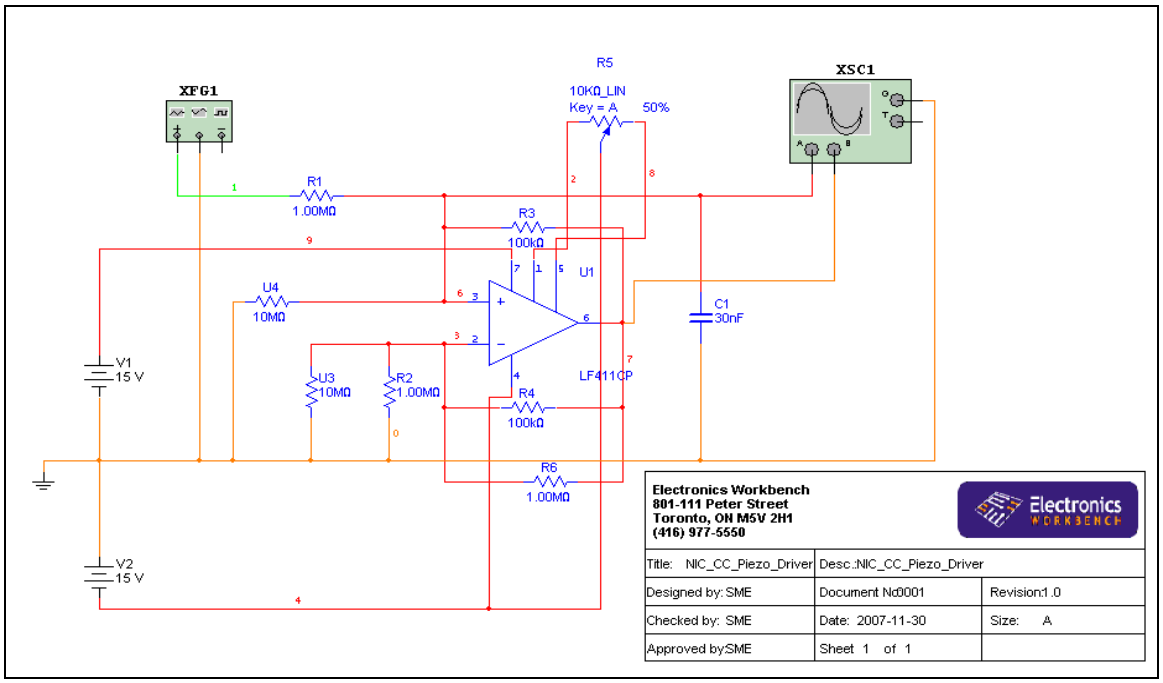


*Figure 12. The NIC constant-current piezo-driver circuit provides a ~ 0.91MΩ negative resistance which nearly completely cancels the 1.0 MΩ coupling resistance. The cancellation of the coupling resistance allows the function generator/voltage amplifier to act as an near-ideal current generator.*

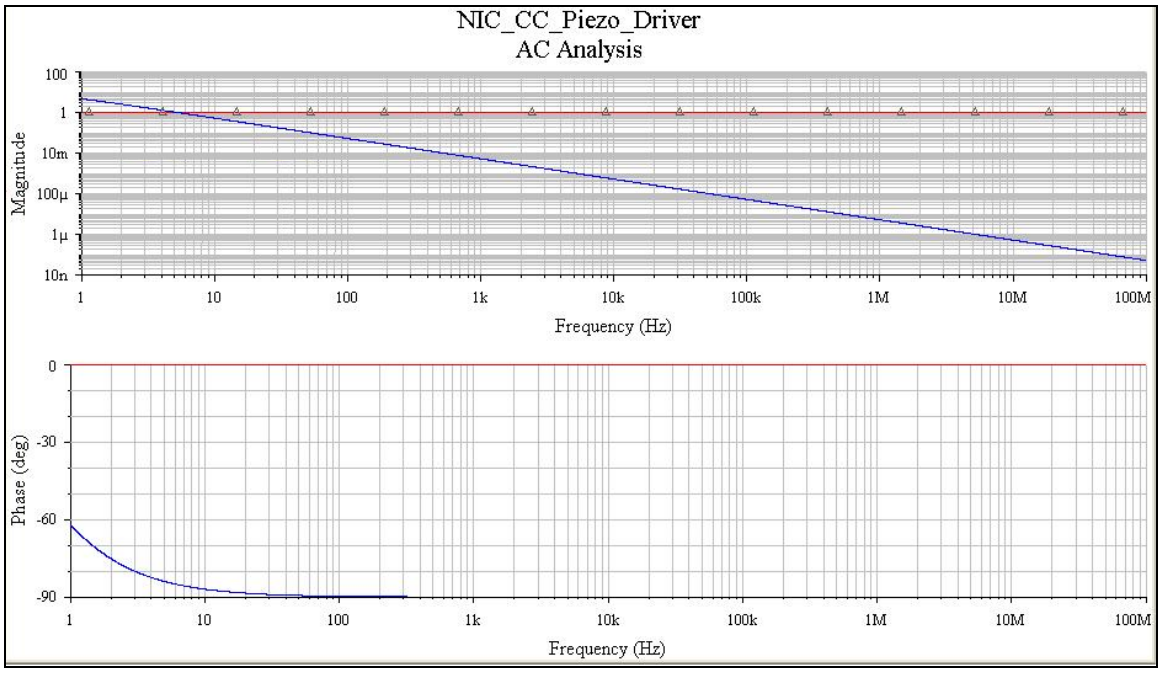


*Figure 13. Voltage gain and phase plots of the NIC constant-current piezo-driver circuit on a logarithmic frequency scale. The blue line represents the output of the NIC constant-current piezo-driver circuit.*

Once the piezoelectric driver, pressure microphones, and differential microphone particle-velocity sensors have been assembled and installed inside and outside the trumpet mouthpiece, the apparatus is connected to a modified version of the UIUC Physics 498POM PC-based electric guitar pickup/loudspeaker impedance measuring system, shown in Figure 14. This PC-Based DAQ System was developed to measure the electrical impedance of electric guitar pickups and loudspeakers. An interesting aspect of complex acoustical impedance ( $\tilde{Z}_{\text{acoustic}}$ ) is that it can be related to complex electrical impedance ( $\tilde{Z}_{\text{electric}}$ ):

$$\boxed{\tilde{Z}(\boldsymbol{r})_{acoustic} = \frac{\tilde{P}(\boldsymbol{r})}{\tilde{\boldsymbol{U}}(\boldsymbol{r})}} \quad \Leftrightarrow \quad \boxed{\tilde{Z}_{electric} = \frac{\tilde{V}}{\tilde{I}}},$$

where complex the pressure ( $\tilde{P}$ ) is the analogue of complex voltage ( $\tilde{V}$ ) and the complex air flow ( $\tilde{U}$ ) is the analogue of complex electric current ( $\tilde{I}$ ). Therefore, connecting the trumpet/sensors to the electric guitar pickup/loudspeaker impedance measuring system is completely straightforward.

The modified system uses a computer-controlled sinusoidal function generator to set the frequency and amplitude of the piezo-driver, as used in the previous system. The voltage signals produced by the microphones and the air-particle-velocity sensors are individually fed into four SRS-830 DSP lock-in amplifiers, using the sine-wave signal output from the Agilent function generator as a reference to determine phase information. The real and imaginary parts of both the microphone voltages and the u-sensor voltage signals, as output from the SRS-830 Lock-In amplifiers are digitized using eight 12 bit ADC channels on a National Instruments LabPC+ DAQ Card and stored in software arrays.[8]

The computer starts the piezo-driver oscillating at a user-defined frequency and amplitude. Once the pressure microphone and u-sensor voltage data have been digitized (10,000× per frequency point) and stored, the PC increases the piezo-driver frequency by a user-defined step size and the process is repeated. The driving frequency can thus be swept over the entire audio frequency range (20 Hz →20,000 Hz). For the purposes of trumpet input impedance measurements, frequency sweeps were run from 29.5 Hz to 4030.5 Hz, using a 1-Hz step size for high-resolution plots. The air in the tubing coupling to higher-order vibrational modes other than the longitudinal mode at frequencies higher than 3000 Hz limits the usefulness of performing frequency scans up to 20,000 Hz. Each run of the program took approximately 9 hours, since there was a multiple second wait

for the outputs of the four lock-in amplifiers to asymptotically settle to their final values. Once the DAQ program had been run, the results could be plotted on 21+ separate on-line graphs (Re(Z) vs. f, Re(I) vs. f, Re(P) vs. f, Re(U) vs. f, etc…) and the data written out to a text-based file for offline analysis.[8]

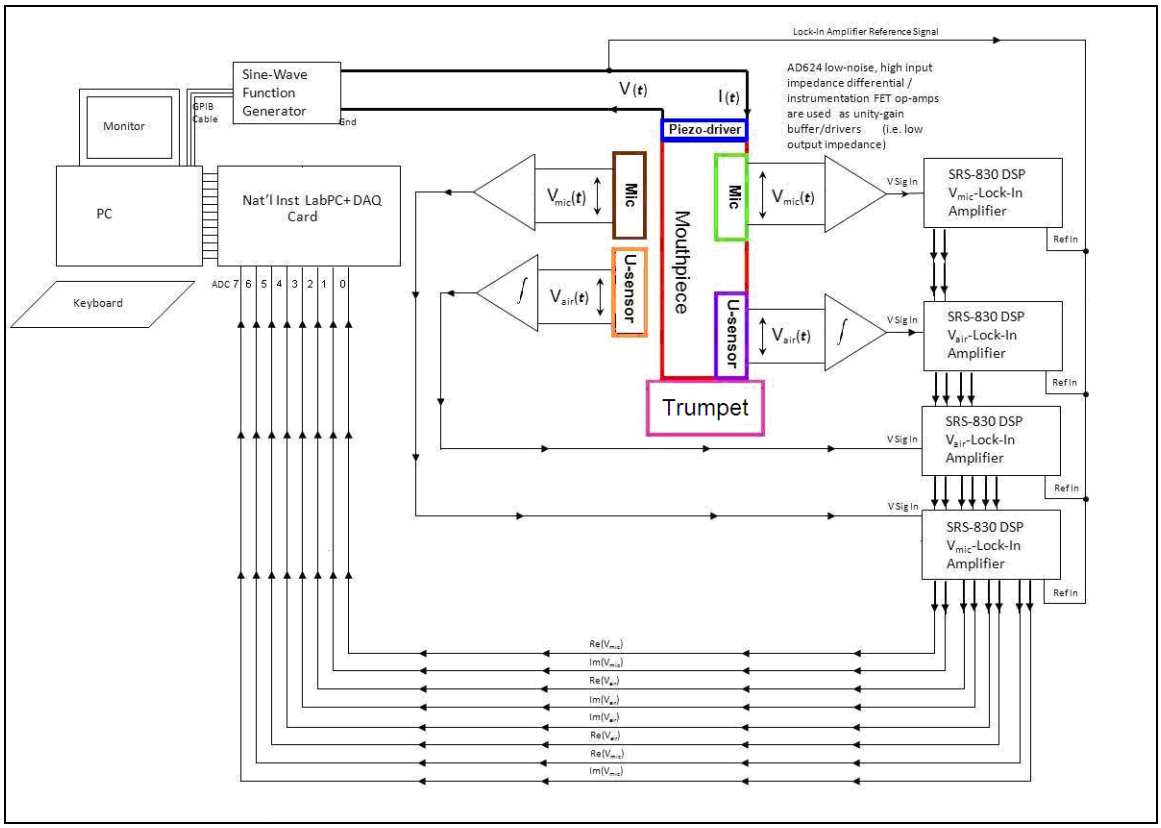


*Figure 14. Modified UIUC Physics 498POM PC-Based Pickup Impedance Measuring System. PC records the average of 10,000 digitizations of each voltage measurement from the microphones and the u-sensors at a given frequency. The calculated impedance over a range of frequency is plotted along with 20+ other online plots.*

To calibrate the phase response of the piezo-transducers, the pressure microphones, and the particle-velocity microphones, frequency scans were run on the "simplest" musical instrument, a standing wave tube. The same pressure and air-particle-velocity microphones that were developed for the trumpet and the same type

of piezo-transducer were used. With a standing wave tube of known dimensions, the complex pressure and particle velocity can be investigated, and relevant phase corrections can be made for each plot. A detailed discussion of the phase corrections is contained in Appendix II.

The absolute calibration of the responses of the pressure and particle-velocity microphones was accomplished using an Agilent 33220A function generator, a Peavey solid-state amplifier with loudspeaker, and an EXTECH 407768 SPL meter (C-weighting) in far-field conditions at 94.0 dB. The sensitivities of the internal and external Knowles Acoustics pressure microphones were measured to be $S_{p1}$ = 294.00 mV/Pa (rms) and $S_{p2}$ = 353.55 mV/Pa (rms) respectively at $f$ = 1 kHz. The sensitivity of the RadioShack and Knowles Acoustics particle-velocity microphones was measured to be $S_{u\text{-}RS}$ = 328.10 mV/Pa$^*$ (rms) and $S_{u\text{-}KA}$ = 339.41 mV/Pa$^*$ (rms) respectively (1 Pa$^*$ = 2.4 mm/s). The microphone sensitivities were determined to ~10% accuracy.

# IV. Results and Discussion

The results discussed in this section, unless explicitly stated, refer to a Bach Omega Bb trumpet with all valves open. As discussed earlier, pressure and particle velocity microphones were placed just outside the mouthpiece to determine if interior vibrations were affecting the air outside the instrument. The raw pressure and particle velocity data both inside and outside the mouthpiece are shown in Figure 15. As the external pressure has been scaled by a factor of 100×, there appears to be a minimal correlation between the internal and external pressure and particle velocity. This result explicitly confirms the decoupling of the air vibrations as being due to the piezo-

transducer's stiffness, thereby not allowing internal vibrations to affect external vibrations.

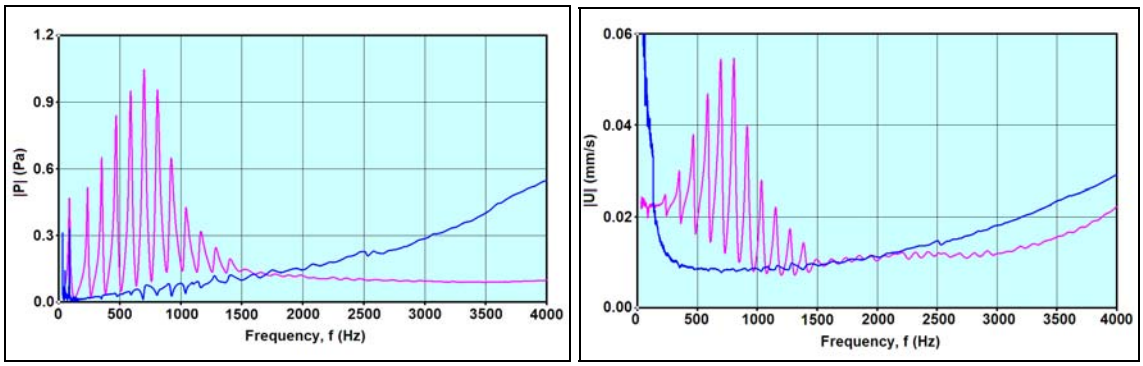


*Figure 15. Pressure (left) and particle velocity data (right). The smooth lower line on each plot represents data taken with the exterior microphones near the piezo transducer. The external pressure (blue) for the left plot has been scaled up by a factor of 100×. The peaks measured with the interior microphones are essentially undetected by the exterior microphones.*

Plots of the real (in-phase) component of internal pressure and the external pressure near the bell of the trumpet as a function of frequency are shown in Figure 16. It is interesting to note that while the real component of the internal pressure stays positive throughout the frequency range, the real component of the external pressure changes phase from peak to trough.

Plots of the imaginary (90° out-of-phase) component of the internal and near-bell external pressure as a function of frequency are shown in Figure 17. It is interesting to note that both the internal and external imaginary component of the complex pressure change phases from peak to trough.

The magnitude of the internal and near-bell external pressure is calculated by taking the square root of the sum of the squares of the real and imaginary data,

$\boxed{|\tilde{p}| \equiv \sqrt{\mathrm{Re}^2\{\tilde{p}\} + \mathrm{Im}^2\{\tilde{p}\}}}$. Plots of the magnitude of the internal and external pressure as a function of frequency are shown in Figure 18. The data for the external pressure detected near the bell of the trumpet are scaled up by a factor of 10 such that both plots can be shown on the same graph. The frequencies of the peaks of the internal and external pressure closely match each other throughout most of the pressure spectrum. The pressure peaks begin to die out around 1500 Hz, thus, barring extremely low values of particle velocity beyond 1500 Hz, playable notes beyond 1500 Hz are unlikely for the trumpet. The frequencies at which pressure peaks occur are close to the frequencies a trumpet can produce, but the particle velocity data is still needed to determine the exact frequency values for a trumpet.

Plots of the phase, $\boxed{\varphi_p \equiv \tan^{-1}\left(\mathrm{Im}\{\tilde{p}\}/\mathrm{Re}\{\tilde{p}\}\right)}$, of the internal and near-bell external pressure as a function of frequency are shown in Figure 19.

Plots of the internal and external Im(P) versus Re(P) in the complex plane is shown in Figure 20. As noted earlier, since the internal Re(P) stayed positive and the Im(P) alternated phase from peak to trough, the internal Im(P) versus Re(P) is confined to the first and fourth quadrants of the complex plane. Both the external Re(P) and Im(P) alternated phase from peak to trough, thus the external Im(P) versus Re(P) is present in all four quadrants of the complex plane.

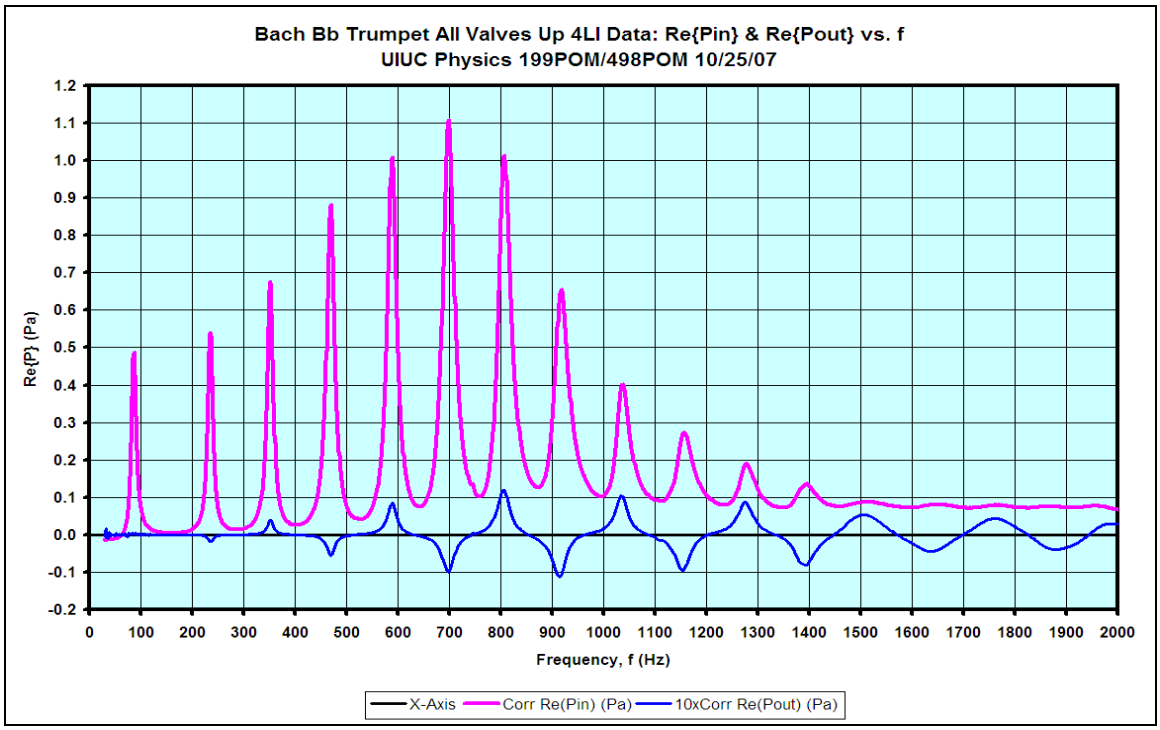


*Figure 16. Real component of the internal (pink) and near-bell external (blue) pressure spectrum (in Pa) up to a frequency of 2000 Hz. The external pressure has been scaled up by a factor of 10 in order to be able to show both plots clearly on the same graph.*

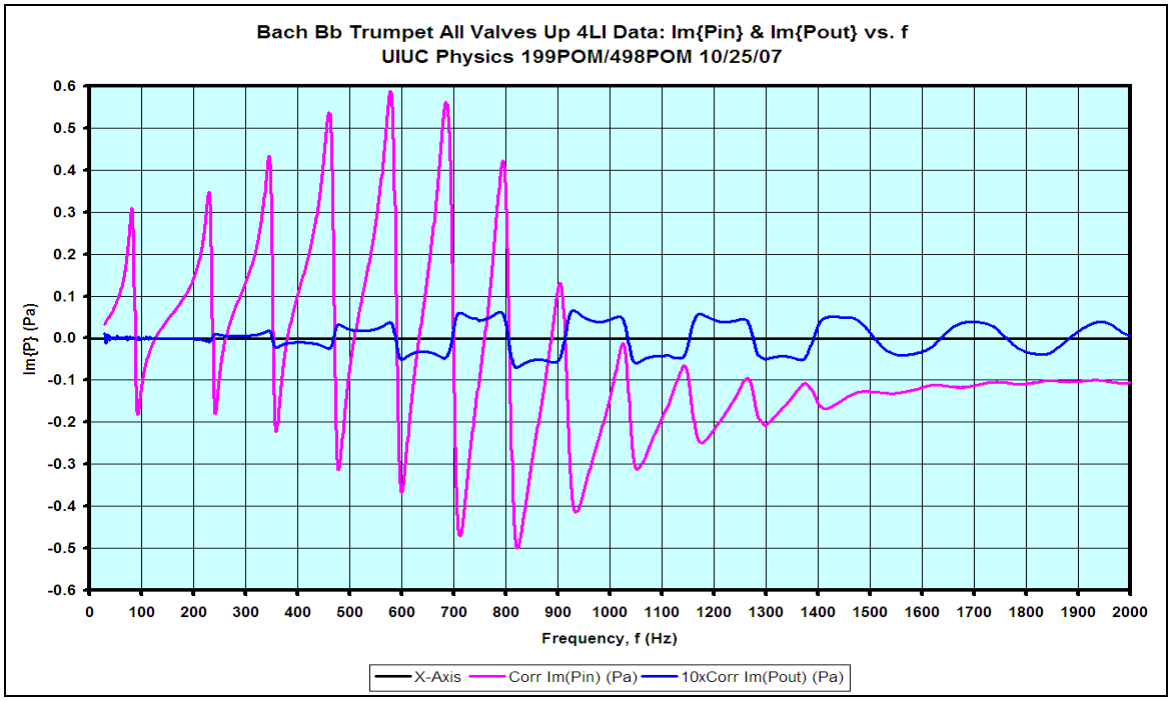


*Figure 17. Imaginary component of the internal (pink) and near-bell external (blue) pressure spectrum (in Pa) up to a frequency of 2000 Hz. The external pressure has been scaled up by a factor of 10 in order to be able to show both plots clearly on the same graph.*

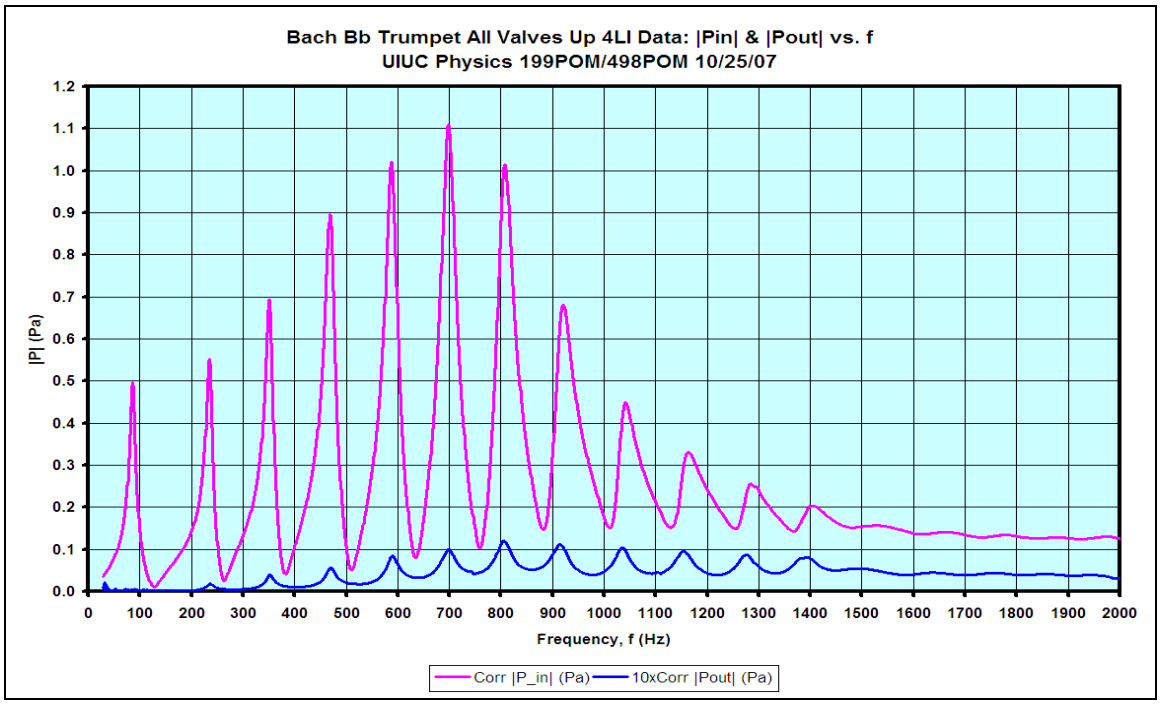


*Figure 18. Internal (pink) and near-bell external (blue) pressure spectrum (in Pa) of a Bb trumpet with all valves open up to a frequency of 2000 Hz. The external pressure has been scaled up by a factor of 10 in order to be able to show both plots clearly on the same graph.*

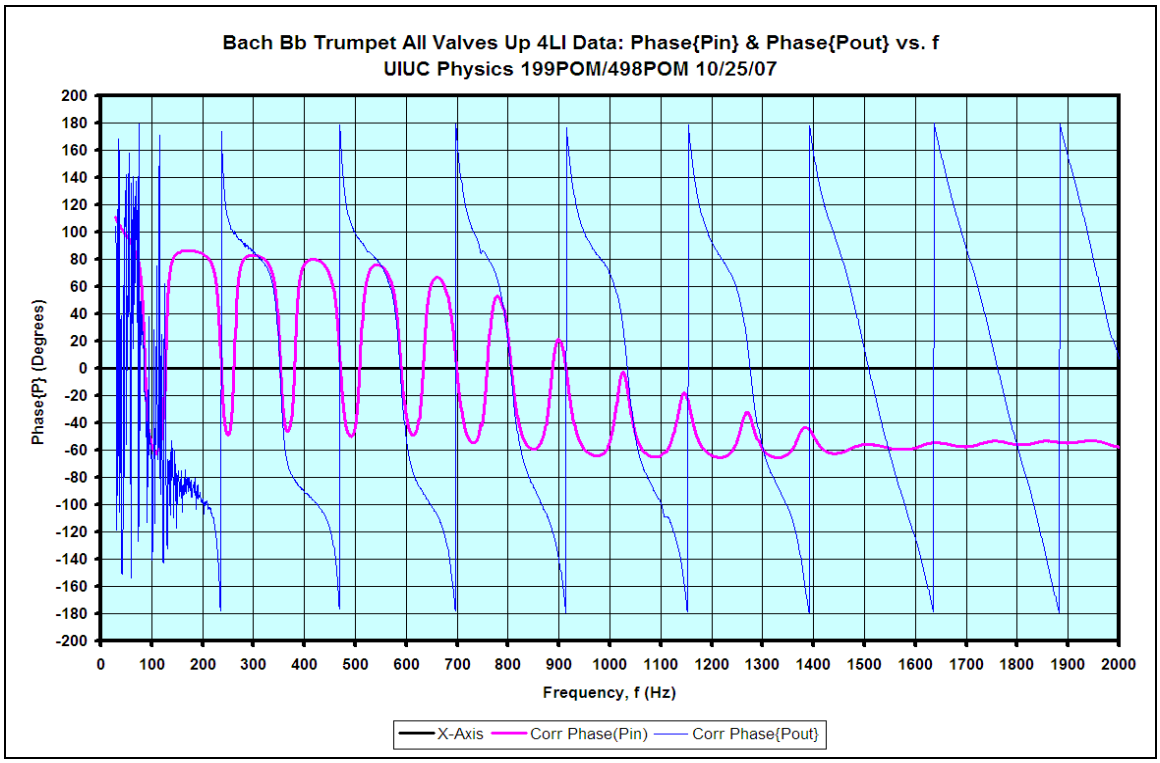


*Figure 19. Phase (in degrees) of the internal (pink) and external (blue) pressure as a function of frequency.*

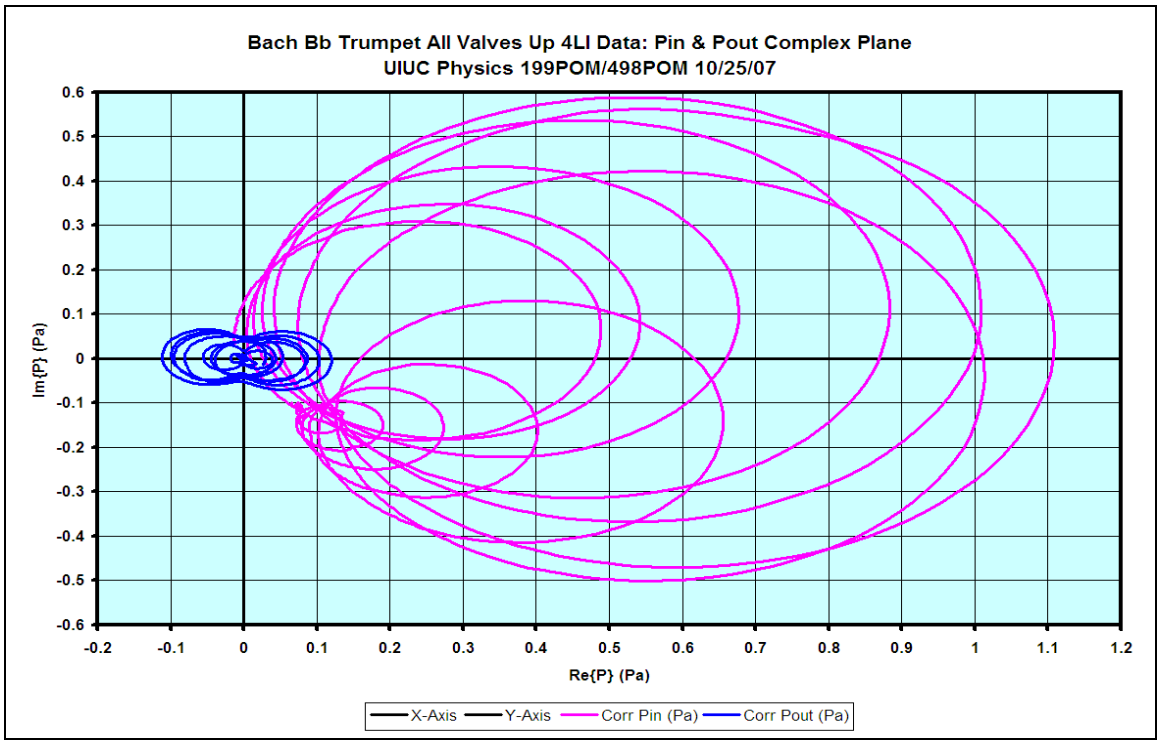


*Figure 20. Internal (pink) and external (blue) Im(p) versus Re(p) (in Pa) on the complex plane.*

Plots of the real component of the internal and near-bell external particle velocity as a function of frequency are show in Figure 21. It is interesting to note that while the real component of the internal particle velocity stays negative throughout the frequency range, the real component of the external particle velocity changes phase from peak to trough in the complex plane.

Plots of the imaginary components of the internal and near-bell external particle velocity as a function of frequency are shown in Figure 22. It is interesting to note that both the internal and external imaginary component of the complex particle velocity change phases from peak to trough.

The magnitude of the particle velocity vector in the complex plane is $\boxed{|\tilde{\boldsymbol{u}}| \equiv \sqrt{\mathrm{Re}^2\{\tilde{\boldsymbol{u}}\} + \mathrm{Im}^2\{\tilde{\boldsymbol{u}}\}}}$. Plots of the magnitude of the internal and near-bell external particle velocity (in mm/s) as a function of frequency is shown in Figure 23. The particle-velocity microphones are particularly susceptible to *1/f* ventilation noise below ~100 Hz. The external particle-velocity microphone exhibits a greater tendency to be hampered by *1/f* noise because the microphone is much more exposed to extraneous airflow than the internal particle-velocity microphone enclosed inside the mouthpiece.

As was the case with the trumpet's internal/external pressure plot, the internal/external particle velocity peaks are also closely matched. The frequencies of these particle velocity troughs, while close to the frequencies of the pressure peaks and the desired frequencies of the trumpet, do not exactly match either of those values. Once again, the troughs of the particle velocity plot start to die out beyond 1500 Hz which supports the upper limit of playable trumpet notes to be ~1500 Hz.

Plots of the phase of the internal and near-bell external particle velocity, $\boxed{\varphi_u \equiv \tan^{-1}\left(\mathrm{Im}\{\tilde{\boldsymbol{u}}\}/\mathrm{Re}\{\tilde{\boldsymbol{u}}\}\right)}$, as a function of frequency are shown in Figure 24.

Plots of the internal and external Im(**U**) versus Re(**U**) in the complex plane is shown in Figure 25. As noted earlier, since the internal Re(**U**) stayed negative and the Im(**U**) alternated phase from peak to trough, the internal Im(**U**) versus Re(**U**) is confined to the second and third quadrants of the complex plane. Both the external Re(**U**) and Im(**U**) alternated phase from peak to trough, thus the external Im(**U**) versus Re(**U**) is present in all four quadrants of the complex plane.

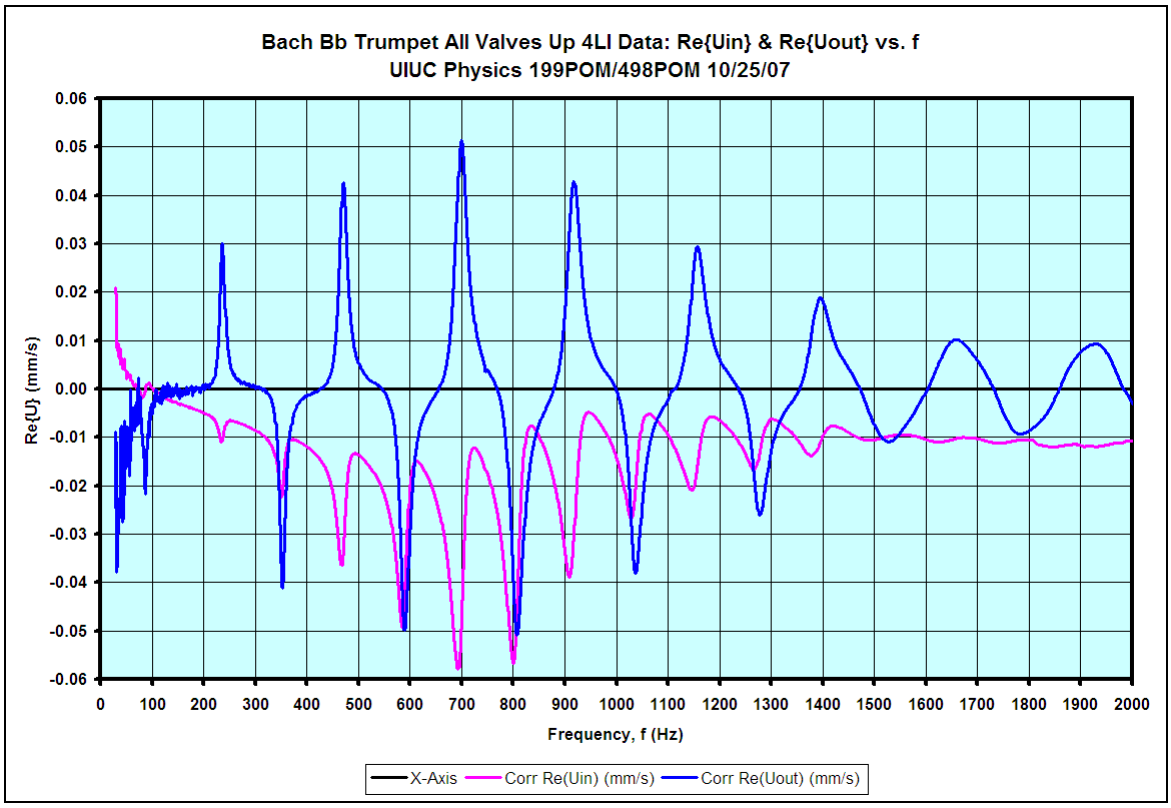


*Figure 21. Real component of the internal (pink) and near-bell external (blue) particle velocity spectrum (in mm/s) up to a frequency of 2000 Hz.*

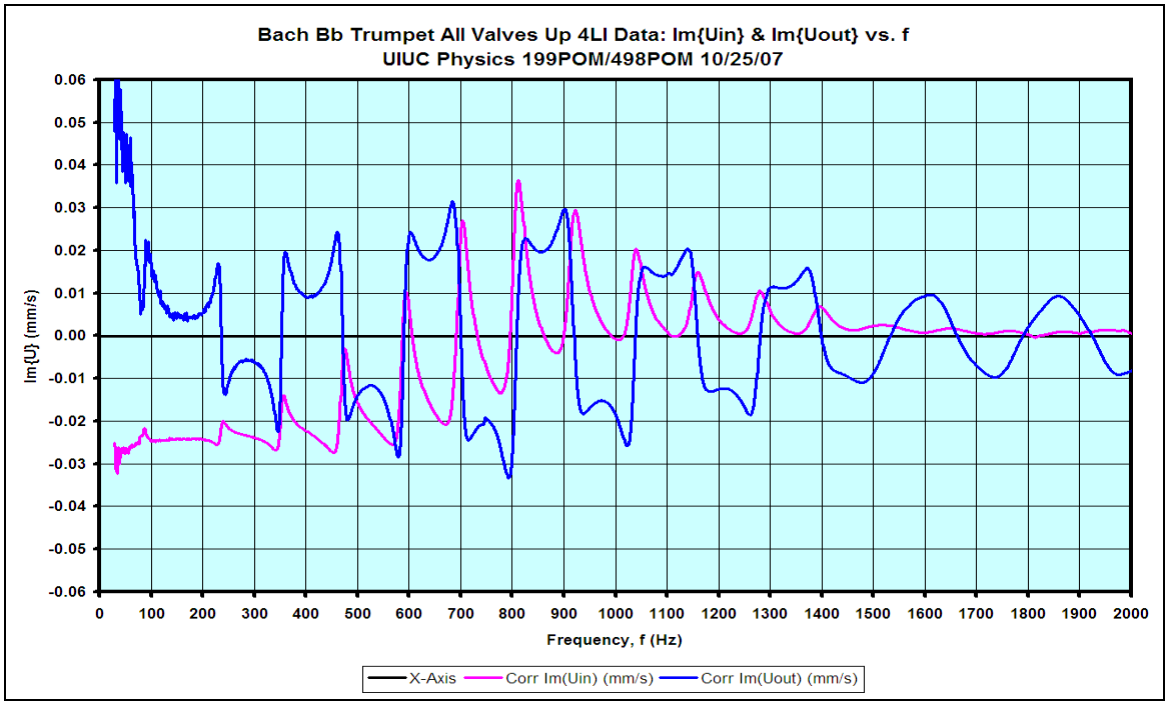


*Figure 22. Imaginary component of the internal (pink) and near-bell external (blue) particle velocity spectrum (in mm/s) up to a frequency of 2000 Hz.*

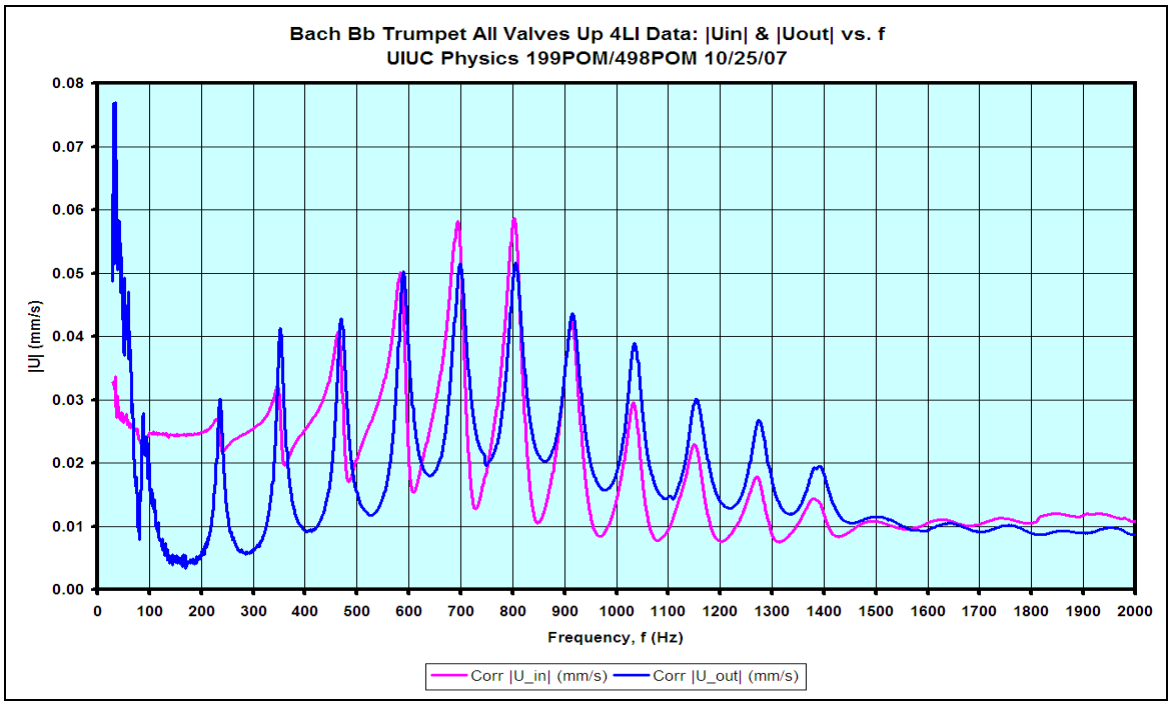


*Figure 23. Internal (pink) and external (blue) particle velocity (in mm/s) of a Bb trumpet with all valves open up to a frequency of 2000 Hz. The peaks and dips of the external particle velocity below ~100 Hz are hampered by 1/f noise from the ventilation system in the room where the experiment was carried out, while the internal particle velocity is unaffected.*

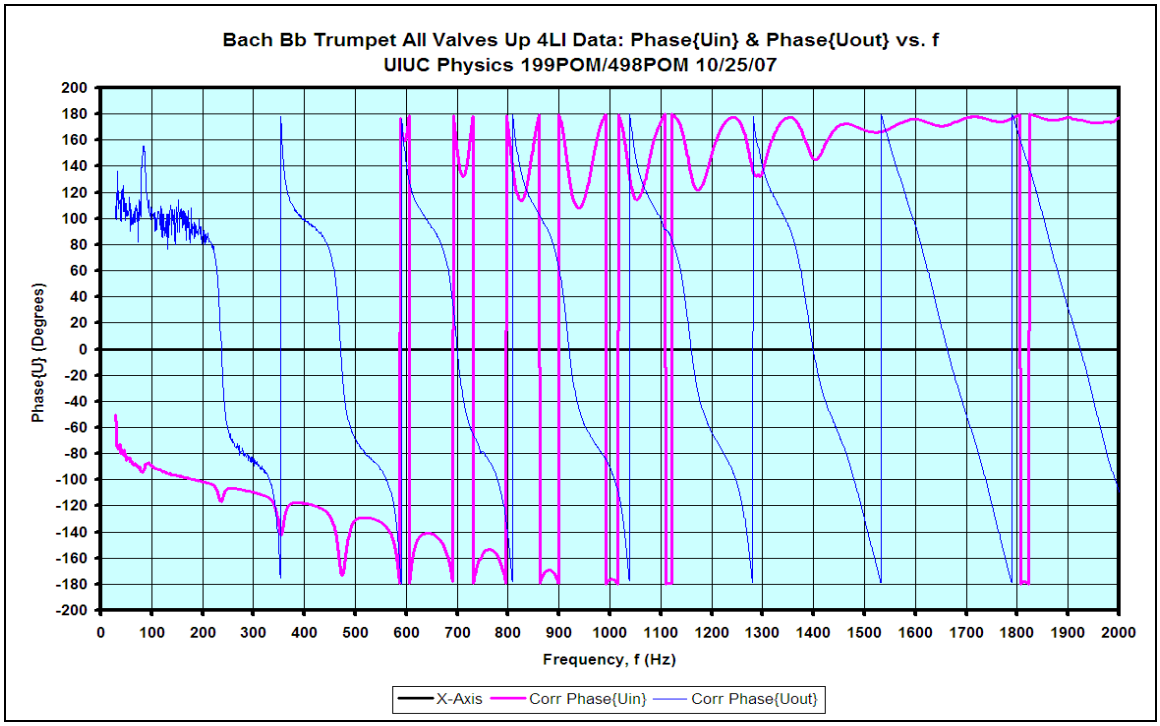


*Figure 24. Plots of the phase (in degrees) of the internal and near-bell external particle velocity as a function of frequency.*

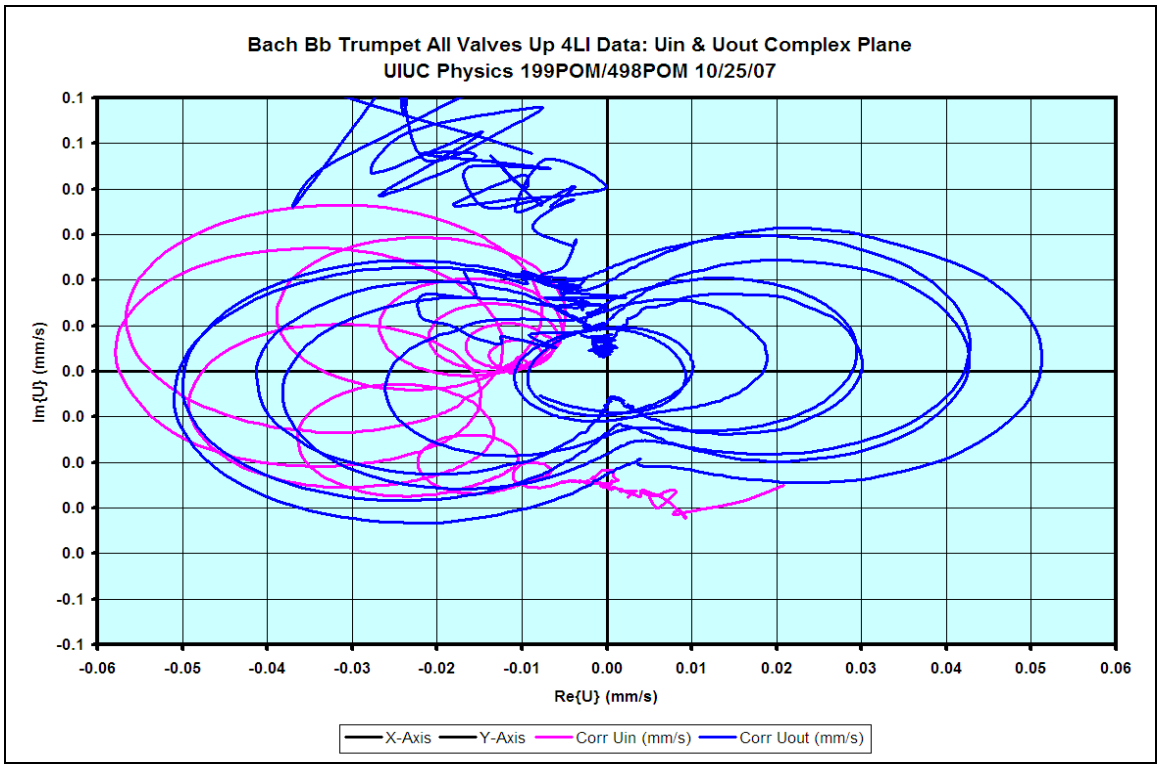


*Figure 25. Internal (pink) and external (blue) Im(**u**) versus Re(**u**) (in mm/s) on the complex plane.*

The quotient of the pressure and the particle velocity gives the impedance spectra. The real component of the input and output impedance, $\boxed{\mathrm{Re}\{Z\} = (p_r u_r + p_i u_i)/u^2}$, where $\boxed{u^2 = u_r^2 + u_i^2}$ as a function of frequency is shown in Figure 26. It is interesting to note that majority of the peaks of the real component of both the output and input impedance stay negative throughout the range of frequency and thus does not experience a phase shift in the complex plane.

The imaginary component of the input and output impedance, $\boxed{\mathrm{Im}\{Z\} = (p_i u_r - p_r u_i)/u^2}$, as a function of frequency is shown in Figure 27. The imaginary component of the input impedance changes phase from peak to trough in the

complex plane while the imaginary component of the output impedance stays positive and thus does not experience a phase shift in the complex plane.

The magnitude of the impedance vector, $\boxed{\left|\tilde{\boldsymbol{Z}}\right| \equiv \sqrt{\mathrm{Re}^2\left\{\tilde{\boldsymbol{Z}}\right\} + \mathrm{Im}^2\left\{\tilde{\boldsymbol{Z}}\right\}}}$, in the complex plane as a function of frequency is shown in Figure 28.

Plots of the phase of the magnitude input and output impedance, $\boxed{\varphi_z \equiv \tan^{-1}\left(\mathrm{Im}\left\{\tilde{\boldsymbol{Z}}\right\} \Big/ \mathrm{Re}\left\{\tilde{\boldsymbol{Z}}\right\}\right)}$, as a function of frequency are show in Figure 29.

Plots of the input and output Im(**Z**) versus Re(**Z**) in the complex plane is shown in Figure 30. As noted earlier, the real component of the input stayed primarily negative while the imaginary component changed phase from peak to trough the input impedance thus the input Im(**Z**) versus Re(**Z**) is mostly contained in the second and third quadrants of the complex plane. Since the real and imaginary component of the output impedance stayed either nearly all negative or all positive, respectively, the output Im(**Z**) versus Re(**Z**) is contained nearly entirely in the second quadrant of the complex plane.

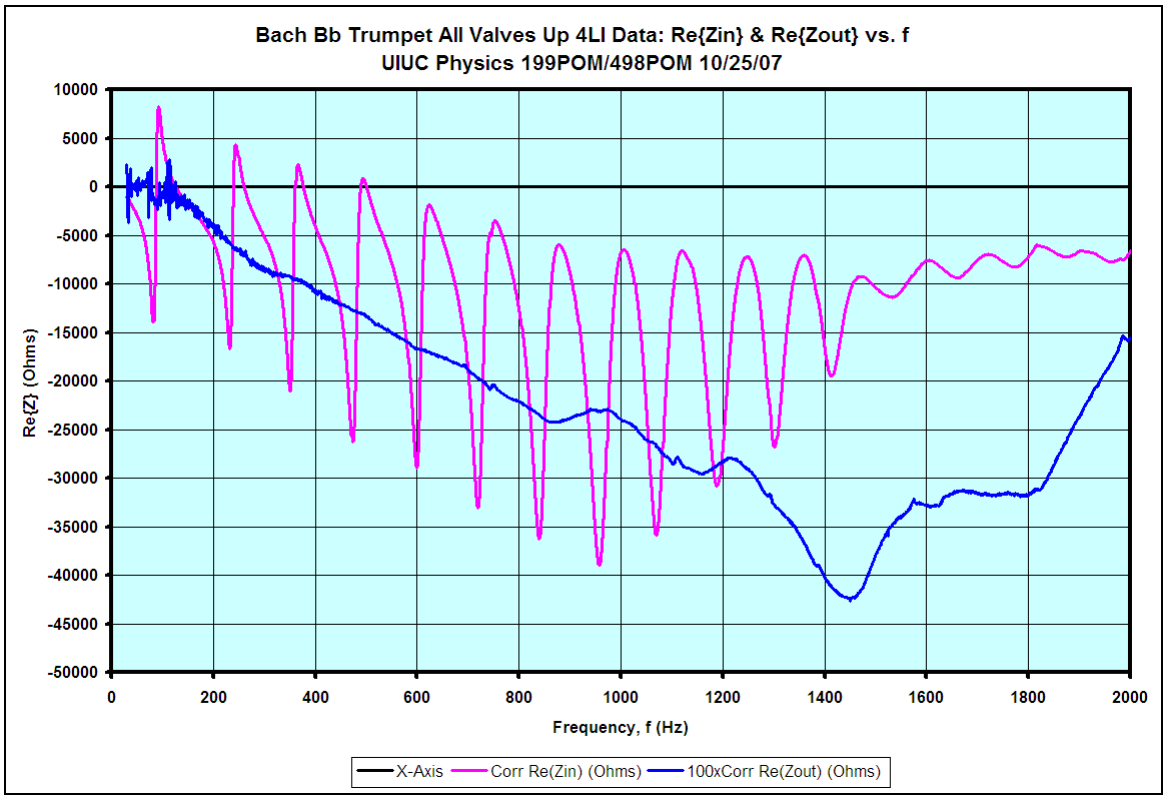


*Figure 26. Real component of the input (pink) and output (blue) impedance spectra (in acoustic ohms) up to a frequency of 2000 Hz. The output impedance has been scaled up by a factor of 10× in order to be able to show both plots clearly on the same graph.*

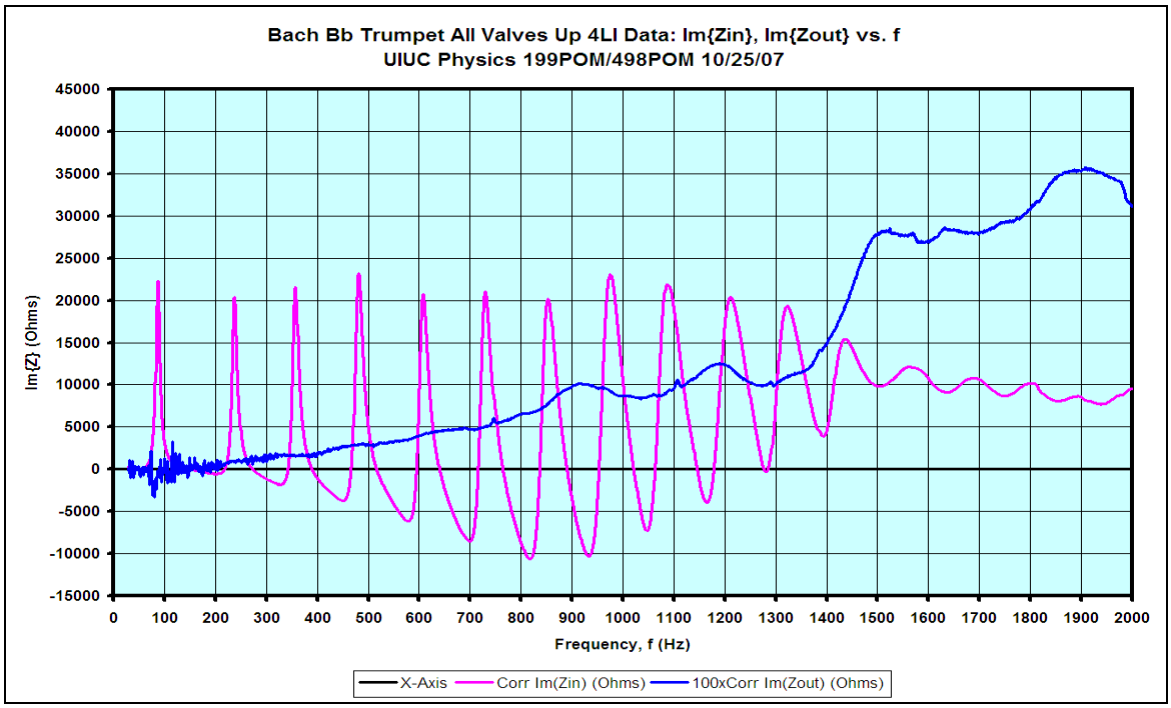


*Figure 27. Imaginary component of the input (pink) and output (blue) impedance spectra (in Ohms) up to a frequency of 2000 Hz. The output impedance has been scaled up by a factor of 10× in order to be able to show both plots clearly on the same graph.*

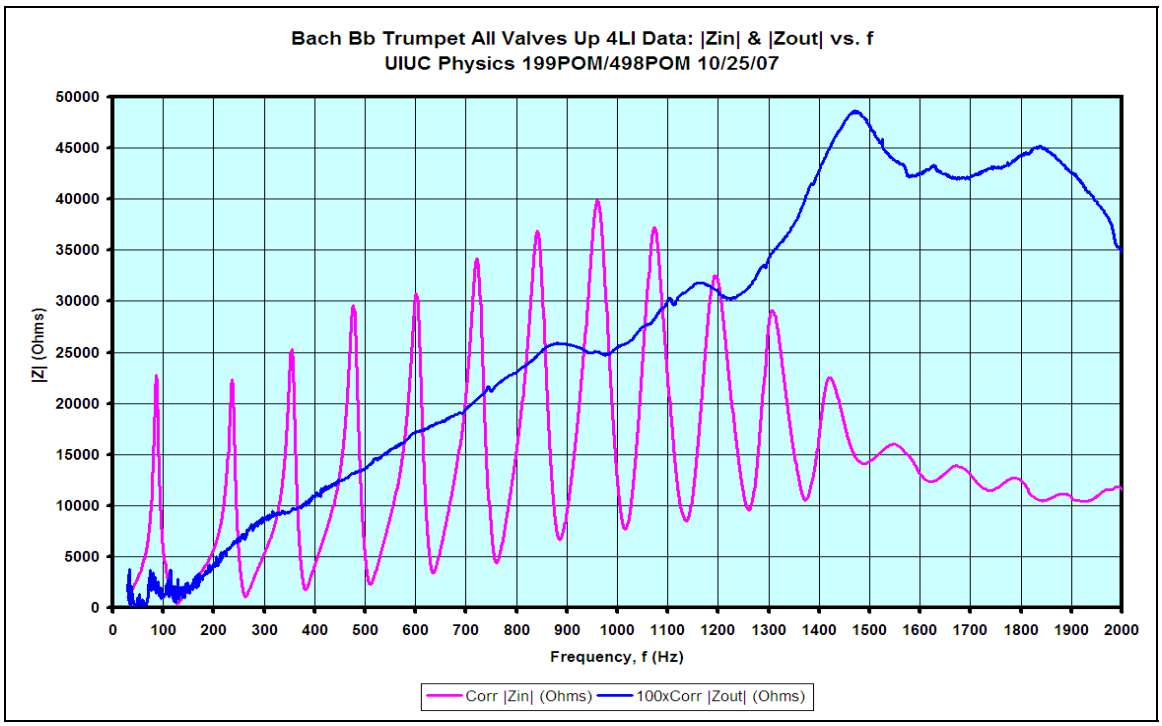


*Figure 28. Input (pink) and output (blue) acoustic impedance spectra (in Ohms) of a Bb trumpet with all valves open up to a frequency of 2000 Hz. The output impedance has been scaled up by a factor of 100×.*

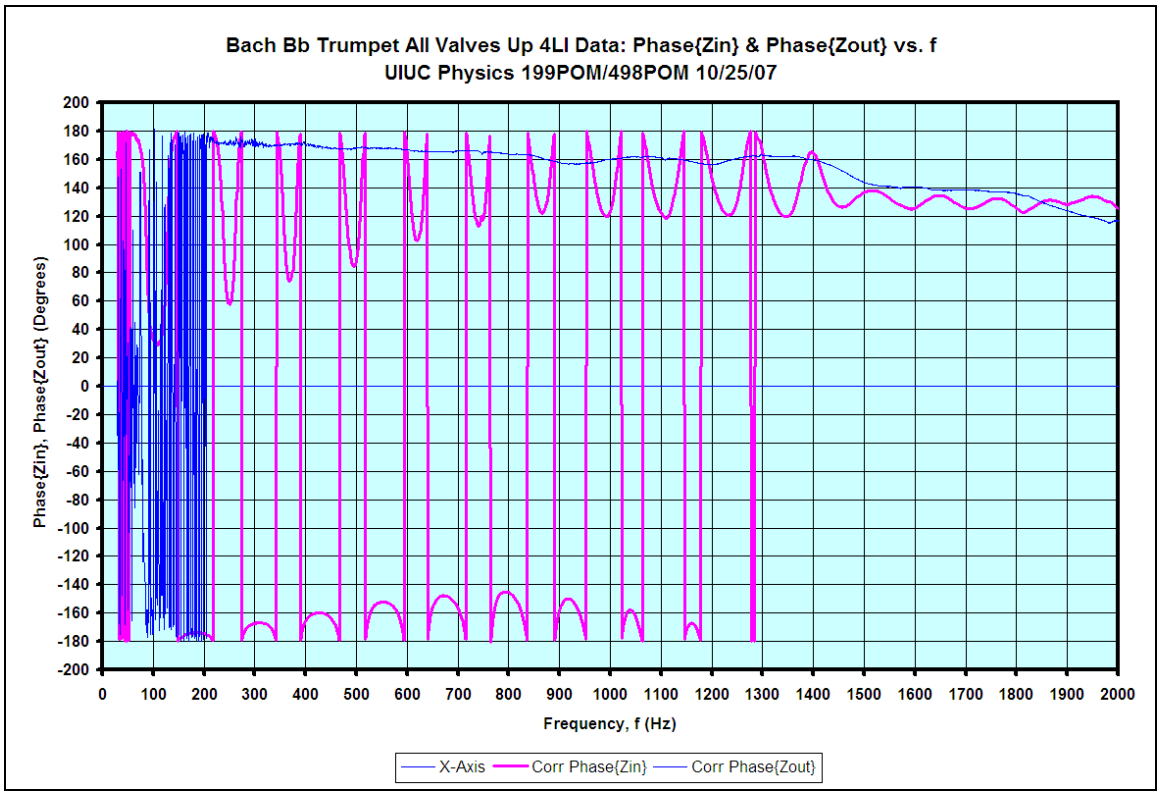


*Figure 29. Plots of the phase (in degrees) of the input (pink) and output (blue) impedance as a function of frequency.*

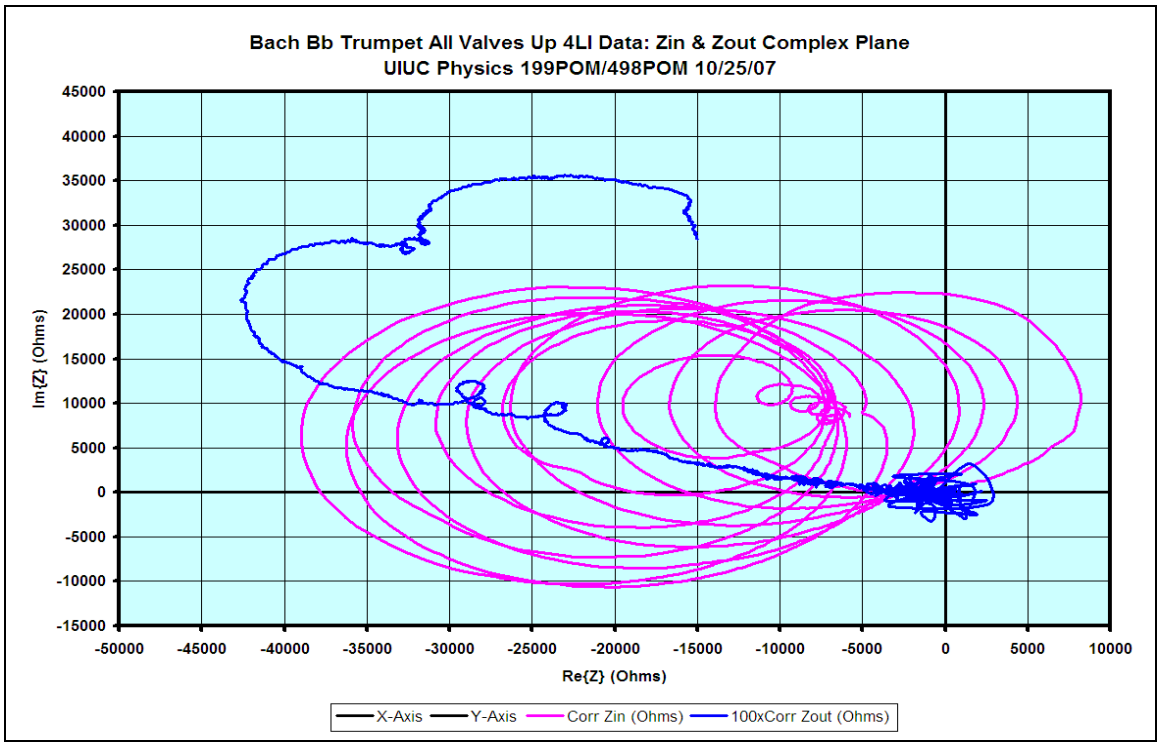


*Figure 30. Internal (pink) and external (blue) Im(**Z**) versus Re(**Z**) (in Ohms) on the complex plane.*

The frequencies at which the peaks of the input impedance occur are shown in Table 1. The measured frequencies of the resonant peaks are systematically higher than the accepted frequency values for a trumpet's notes simply because the trumpet was not tuned prior to it being attached to the experimental apparatus; the main tuning slide was pushed all of the way in. Were a person to play the instrument when the tuning slide was in this position, he would find the notes he produced unpleasantly sharp (frequency shifted up). To correct for this tuning discrepancy, tuned frequency values were found by determining the percent the measured C4 needed to be scaled to match the accepted C4 and applying this scale factor to all measured frequencies. This process retroactively tunes the trumpet. A plot of the % deviation the tuned frequencies are from the accepted frequencies is shown in Figure 31. The measurements for output impedance eventually reaches and stays around 420 acoustic ohms which is close to the accepted value of ~413 acoustic ohms for the impedance of {bone-dry} free air at NTP.

**Deviation from Accepted Frequency Values**

| Note Name | Accepted Freq. (Hz) | Measured Freq. (Hz) | Tuned Freq. (Hz) | % Difference |
|---|---|---|---|---|
| C4 | 233.08 | 236.5 | 233.1 | 0.0% |
| G4 | 349.23 | 354.5 | 349.4 | 0.1% |
| C5 | 466.16 | 477.5 | 470.6 | 1.0% |
| E5 | 587.33 | 601.5 | 592.8 | 1.0% |
| G5 | 698.46 | 721.5 | 711.1 | 1.8% |
| Bb5 | 830.61 | 841.5 | 829.3 | -0.2% |
| C6 | 932.33 | 960.5 | 946.6 | 1.5% |
| D6 | 1046.50 | 1073.5 | 1058.0 | 1.1% |
| E6 | 1174.66 | 1193.5 | 1176.2 | 0.1% |
| Gb6 | 1318.51 | 1307.5 | 1288.6 | -2.3% |

*Table 1. Accepted note frequency values for a Bb trumpet with all valves open, frequency values for measured impedance peaks starting from second peak, and tuned frequency values. The tuned frequency values were found by determining the percent the measured C4 needed to be scaled to match the accepted C4 and applying this scale factor to all measured frequencies. The % difference is the variation between the tuned frequencies and the accepted frequencies.*

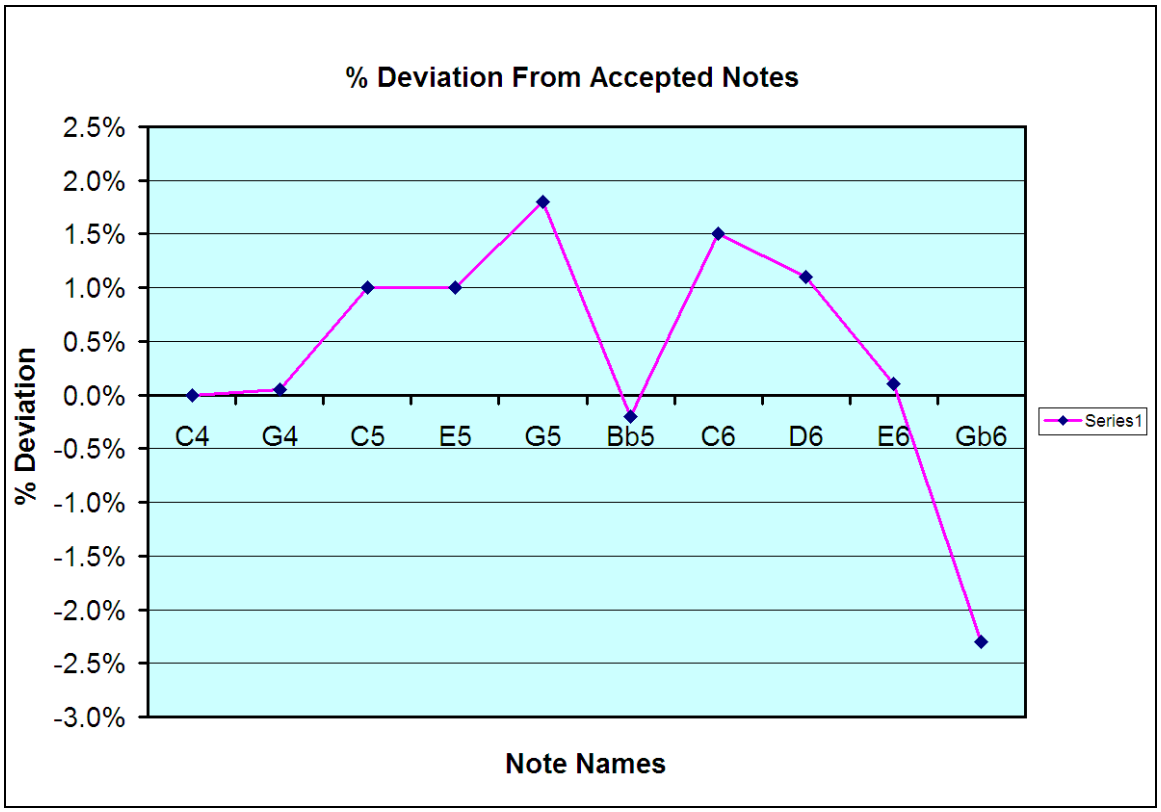


*Figure 31. % Deviation from accepted note frequencies. Tuned frequencies match accepted frequencies to a few %.*

Previously, the unplayablity of the ~117 Hz fundamental frequency of the trumpet was discussed and attributed to the construction of the mouthpiece. Examining the newly presented impedance data shows why the fundamental cannot be easily played. The input impedance data alone implies that the fundamental frequency cannot be played because there is an impedance trough precisely at this frequency value. The construction of the trumpet actually lowers the fundamental peak from ~117 Hz to ~86 Hz. A musician may assume that even though the fundamental at 117 Hz is not available, this lower note at 86 Hz should be playable due to the impedance peak that exists at 86 Hz. The musician would be wrong. Again, impedance peaks indicate frequencies at which most pressure waves are reflected from the interior of the bell to essentially lock lip vibration frequency

to a desired note. Some pressure waves must exit the instrument or sound from the instrument would never propagate to a listener's ear, thereby making concerts painfully boring. In the case of the lowest frequency peak at 86 Hz, the output impedance of the instrument is extremely low. This low external impedance serves to essentially reflect all of the pressure waves back to the player's lips without allowing any sound the exit the instrument.

A similar argument can be applied to the high end frequency limit of notes a trumpet can play. Notice, once the output impedance reaches a value around 420 acoustic ohms the input impedance peaks exhibit a sharp decrease in magnitude. This decrease in magnitude—and, thus, ease of playability of a note—can be attributed to the impedance mismatch, which reflects the pressure waves, suddenly matching with the output impedance. This matching results in scarce pressure wave information being reflected back to the player's lips which inhibits notes to be played.

As discussed earlier, the height of an impedance peak at a specific frequency is directly related to the ease of playability of the note corresponding to that frequency. According to Figure 28, the highest peak occurs at ~960 Hz which corresponds to a C6 on a trumpet. Thus, a C6 should be the "easiest" note to play on the tested trumpet. But, even though the C6 is the "easiest" note to play, the quality of the impedance peak at ~960 Hz is less than at other frequency values. This implies that while a player of the tested trumpet may be able to play the C6, the player will have a greater difficulty keeping that note in tune compared to another note—say E5 at ~601 Hz—with a high quality impedance peak.

We initially set out to determine the input impedance of a Bb trumpet. However, using the same pressure and air particle velocity data, we can additionally determine the longitudinal component of the complex sound intensity (in nW/m$^2$) at the input point and at the output point:

$$\left\langle \tilde{\boldsymbol{I}}(\boldsymbol{r}) \right\rangle = \frac{1}{2}\tilde{P}(\boldsymbol{r}) \cdot \tilde{\boldsymbol{U}}^{*}(\boldsymbol{r}) .$$

Plots of the real part of the time-averaged longitudinal component of the complex sound intensity at the input and output points, $\boxed{\mathrm{Re}\{I\} = p_r u_r + p_i u_i}$, as a function of frequency are shown in Figure 32. It is interesting to note that the real components of both the input and output intensity stay primarily negative through the frequency spectrum and thus exhibit no phase shift.

Plots of the imaginary part of the time-averaged longitudinal component of the complex sound intensity at the input and output points, $\boxed{\mathrm{Im}\{I\} = p_i u_r - p_r u_i}$, as a function of frequency are shown in Figure 33. The imaginary component of the input intensity changes phase in the complex plane from peak to trough while the imaginary component of the output intensity stays positive and thus exhibits no phase shift in the complex plane.

The magnitude of the time-averaged complex longitudinal sound intensity vector at the input and output points, $\boxed{\left|\tilde{\boldsymbol{I}}\right| \equiv \sqrt{\mathrm{Re}^2\left\{\tilde{\boldsymbol{I}}\right\} + \mathrm{Im}^2\left\{\tilde{\boldsymbol{I}}\right\}}}$ as a function of frequency is shown in Figure 34.

Plots of the phase of the input and output time-averaged complex longitudinal sound intensity, $\boxed{\varphi_I \equiv \tan^{-1}\left(\mathrm{Im}\left\{\tilde{\boldsymbol{I}}\right\} \Big/ \mathrm{Re}\left\{\tilde{\boldsymbol{I}}\right\}\right)}$, as a function of frequency are shown in

Figure 35. As discussed concerning the standing wave tube in Appendix III, the plots of the phase of the impedance and intensity as a function of frequency for the trumpet are identical.

Plots of the input and output Im(**I**) versus Re(**I**) in the complex plane is shown in Figure 36. As noted earlier, since the input Re(**I**) stayed negative and the Im(**I**) alternated phase from peak to trough, the input Im(**I**) versus Re(**I**) is confined to the first and fourth quadrants of the complex plane. Both output Re(**I**) and Im(**I**) stay either negative or positive, respectively, throughout the frequency range. Thus the output Im(**I**) versus Re(**I**) is confined to the third quadrant.

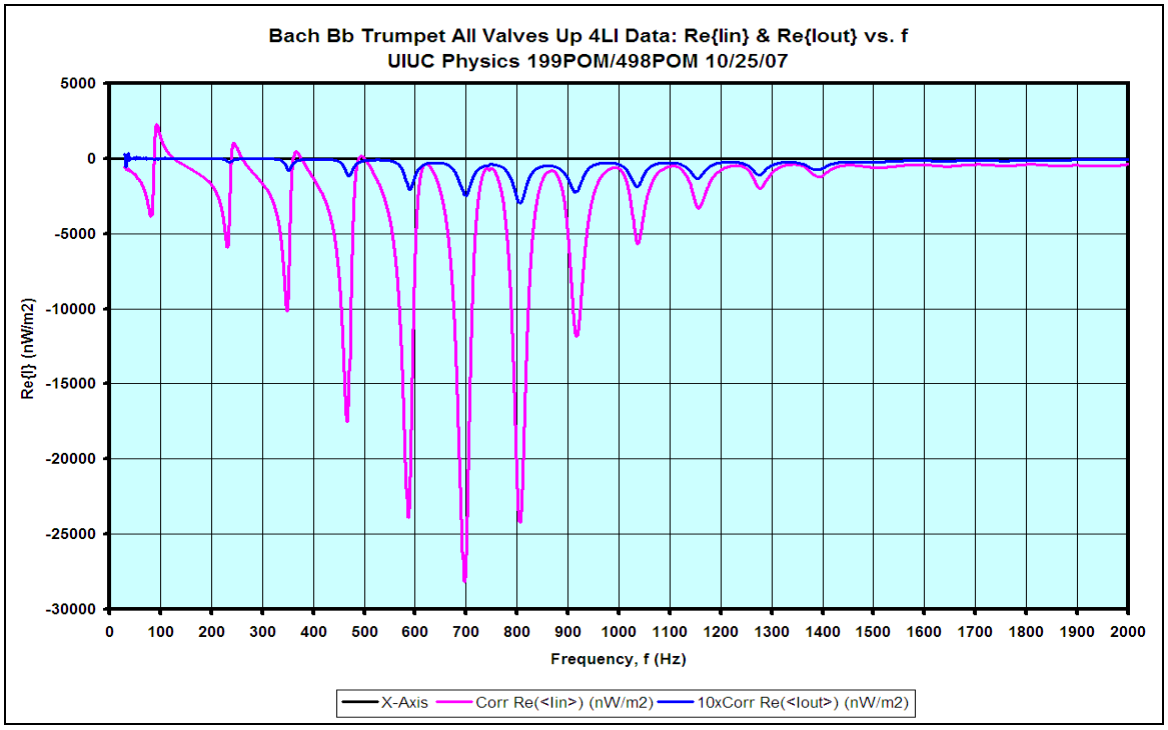


*Figure 32. Real component of the time-averaged sound intensity (in nW/m^2) up to a frequency of 2000 Hz. The output intensity has been scaled up by a factor of 10× in order to be able to show both plots clearly on the same graph.*

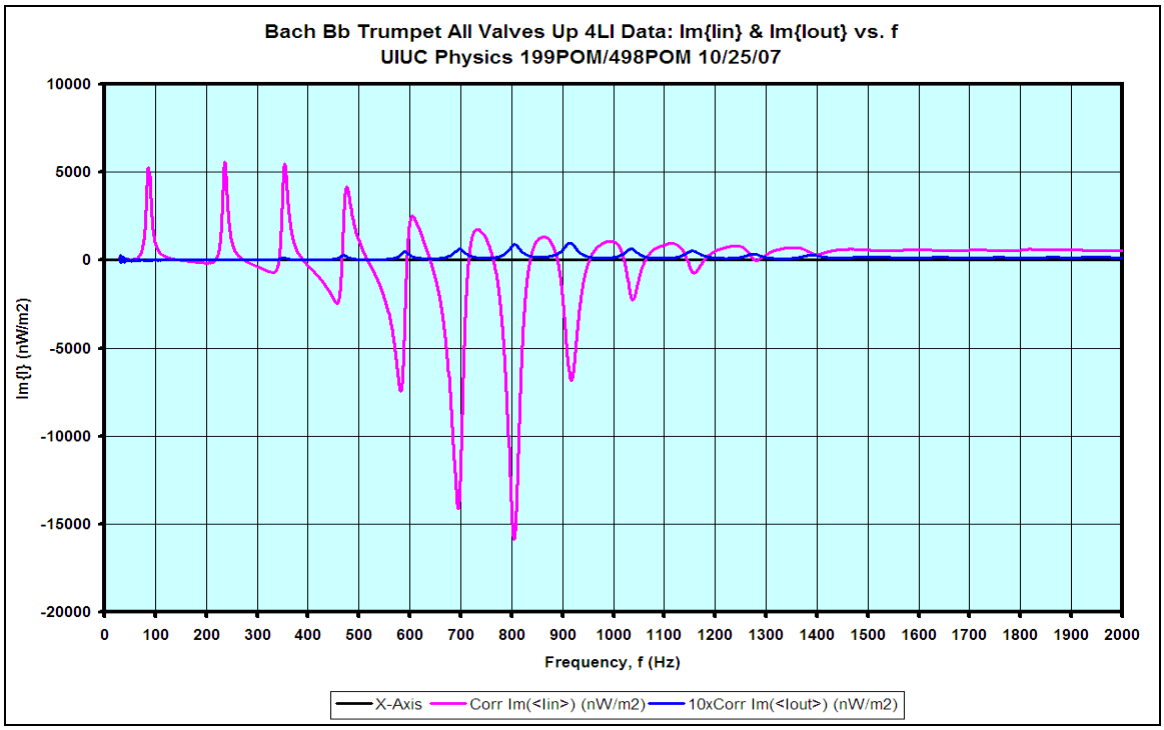


*Figure 33. Imaginary component of the time-averaged sound intensity (in nW/m^2) up to a frequency of 2000 Hz. The output intensity has been scaled up by a factor of 10× in order to be able to show both plots clearly on the same graph.*

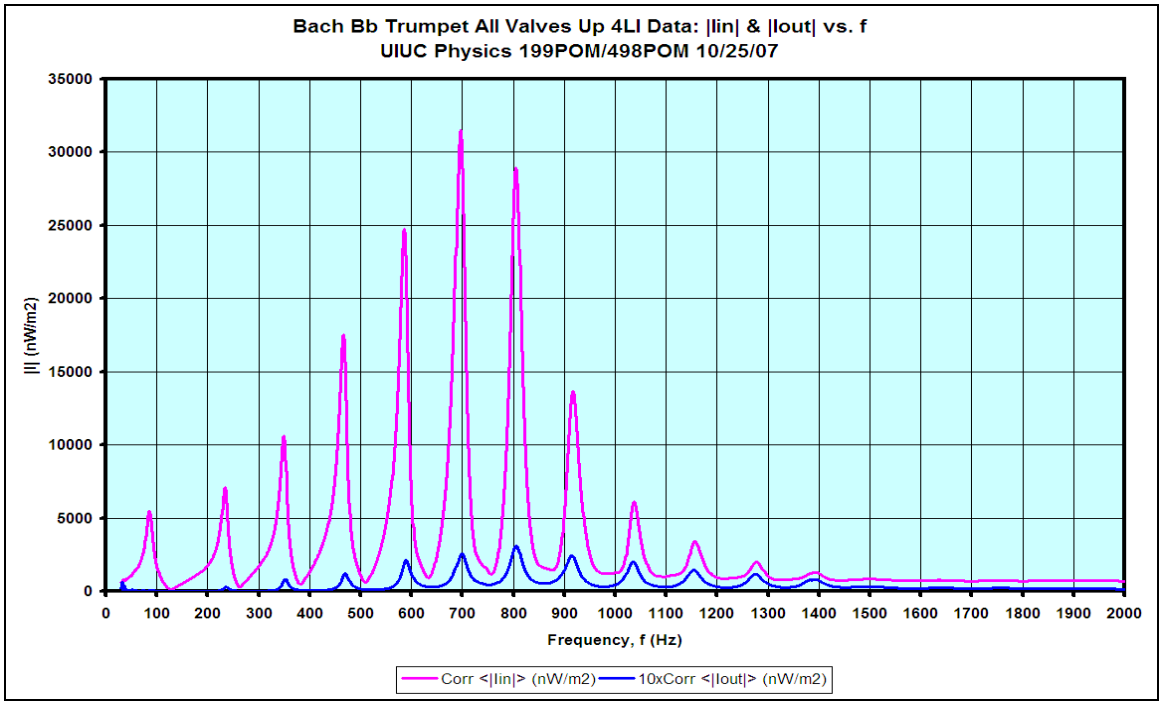


*Figure 34. The time-averaged longitudinal component of the acoustical input (pink) and output (blue) intensity of a Bb trumpet over a range of frequencies up to 2000 Hz. The output intensity has been scaled up by a factor of 10× so both sets of data can be shown on the same plot.*

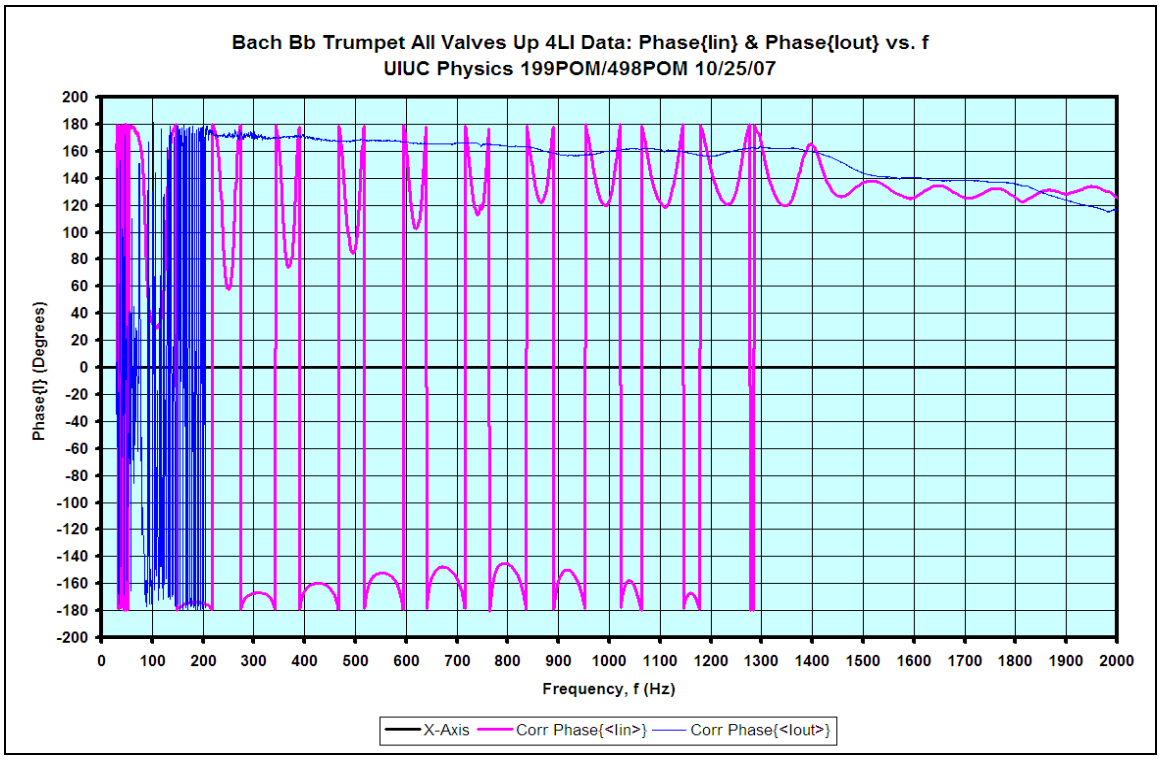


*Figure 35. Phase (in degrees) of the input (pink) and output (blue) longitudinal complex sound intensity as a function of frequency.*

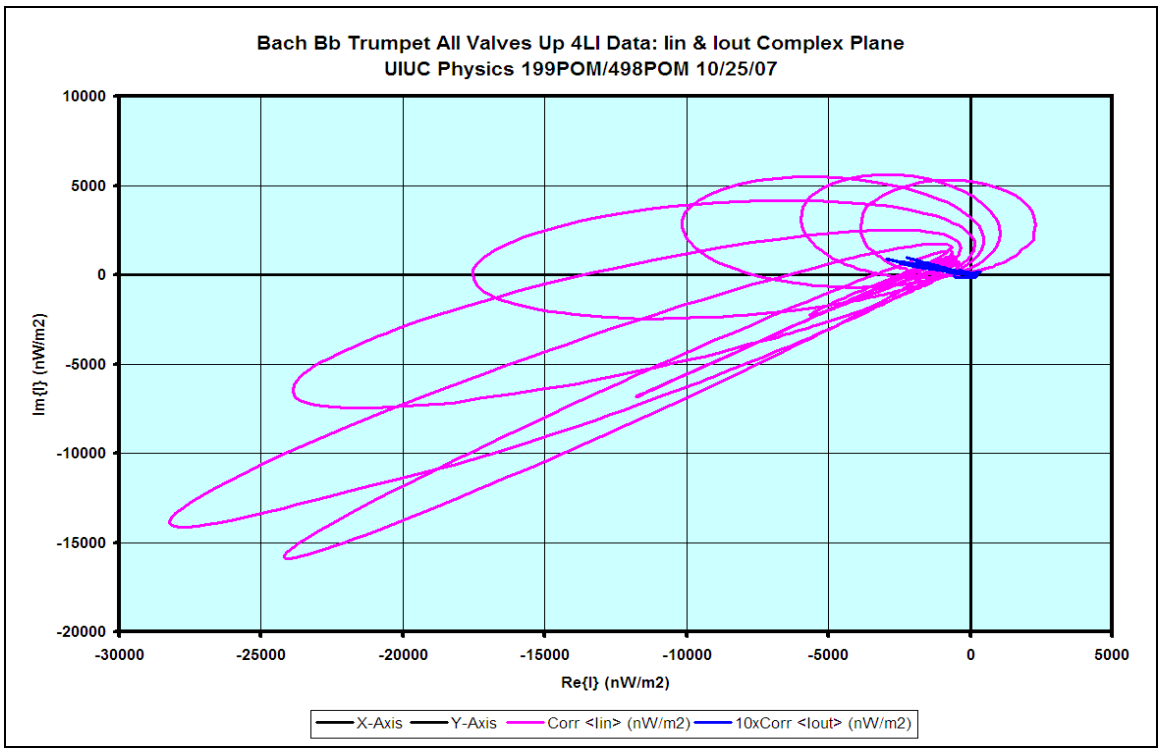


*Figure 36. Internal (pink) and external (blue) Im(**I**) versus Re(**I**) (in nW/m^2) on the complex plane.*

Finally, a plot of the 1-D sound intensity factor (SIF) as a function of frequency is shown in Figure 37. $\boxed{SIF \equiv 100 * \cos(\varphi_I) = 100 * I_r \Big/ \left|\tilde{p}\right|\left|\tilde{\boldsymbol{u}}^*\right| (\%)}$. Since $\boxed{\varphi_I = \varphi_Z = \varphi_p - \varphi_u}$ SIF = 100% (−100%) occurs when $\varphi_I = \varphi_Z = \varphi_p - \varphi_u = 0°(180°)$, respectively.

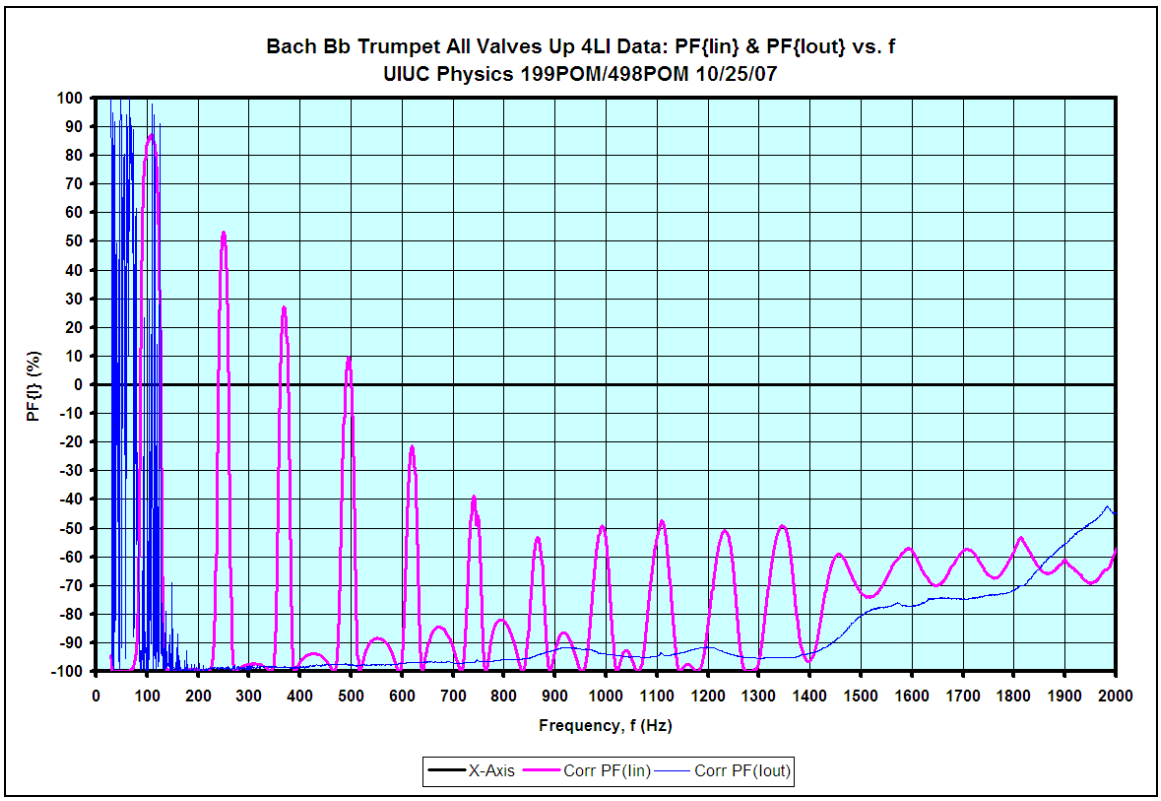


*Figure 37. Internal (pink) and external (blue) sound intensity factor as a function of frequency.*

# V. Conclusions

The goal of this experiment was to develop and implement a method of determining the input and output impedance spectra of a Bb trumpet. Using the techniques described in this paper, these impedance spectra were obtained. The spectra described the behavior of the trumpet, from ease of playing a note to difficulty keeping a note in tune. The results also gave physical reasons why the fundamental frequency of the trumpet is unavailable and why the frequency range of a trumpet can go only so high.

Phase corrected data for the real and imaginary components of both the internal/external pressure and particle velocity have also been obtained. The author at the time this paper was written is unaware of any other source that discusses the complex—i.e. real, imaginary, and phase components of acoustic impedance or intensity inside musical instruments. All previous work has been concerned only with the magnitude of the impedance or intensity spectra.

# VI. Future Work

The process described in this paper produces the input impedance spectrum for one valve combination of the trumpet. While data has been taken for every possible valve combination for the trumpet, the researchers had neither the time nor the patience to present here all phase and magnitude plots for all valve combinations—however, a collection of the input and output impedance spectra for the eight different valve combinations can be found in Appendix IV. A comparison of the real, imaginary, and phase information for the input and output pressure, particle velocity, impedance, and intensity can be carried out by future parties to find what effect the valves themselves have on these values.

While this paper primarily focused on the trumpet, using a pressure sensitive microphone and a newly developed particle velocity sensor makes it possible to measure the complex acoustical impedance and intensity of any instrument or vibrating column of air. The sensor combination can also be used to obtain the acoustical impedance and intensity of free space or an arbitrary sound field.

This technique would be useful for tubular reconstruction of broken instruments or the development of new instruments. By reverse engineering a known impedance spectrum—either custom designed or from a previous measurement on an instrument—the tubing needed to recreate that impedance spectrum can be found thereby creating a new instrument or fixing an old instrument.[9] Since this technique need not apply to musical instruments only, this same method of tubular reconstruction can be applied to any kind of pipe. Knowing where a hole in a pipe is without examining the entire length can be extremely beneficial.

While the integral of the differential pressure signal from the differential microphone yields a signal linearly proportional to the particle velocity, a better way to obtain results is by measuring the particle velocity directly. Prototypes for several candidate particle velocity sensors that have the potential of directly measuring air particle velocity have been developed.

## VII. Acknowledgements

I would like to thank Prof. Steven Errede and Mr. Jack Boparai for their continuing help with this research. I would also like to thank the engineers William Ballad, Bob McDonald, Torey Tomaso, and Tim Wickstrom at Knowles Acoustics for their insights and help concerning the development of our pressure and particle-velocity microphones. Finally, I would like to thank the University of Illinois at Urbana-Champaign Physics Department and the Shell Foundation for their support.